AD-A120 484 NUMERICAL ANALYSIS OF SEMICONDUCTOR DEVICES USING MICROCOMPUTERS(U) WASHINGTON UNIV ST LOUIS MO DEPT OF ELECTRICAL ENGINEERING P S CHEN ET AL. JUL 82 1/2

UNCLASSIFIED TR-82-3-ONR N00014-79-C-0840 F/G 9/1 NL

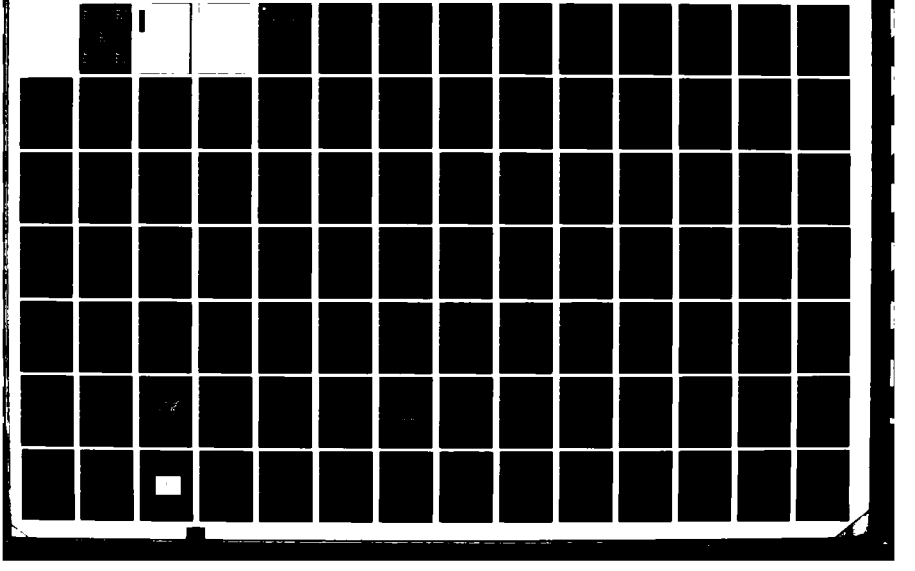

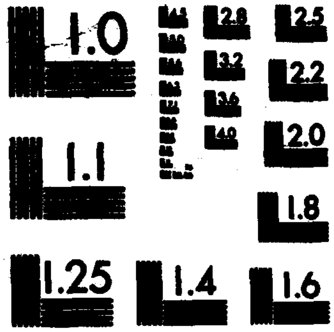

MICROCOPY RESOLUTION TEST CHART
NATIONAL BUREAU OF STANDARDS-1963-A

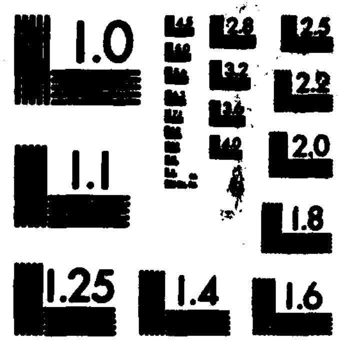

MICROCOPY RESOLUTION TEST CHART
NATIONAL BUREAU OF STANDARDS-1963-A

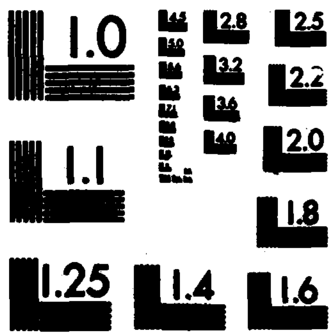

MICROCOPY RESOLUTION TEST CHART
NATIONAL BUREAU OF STANDARDS-1963-A

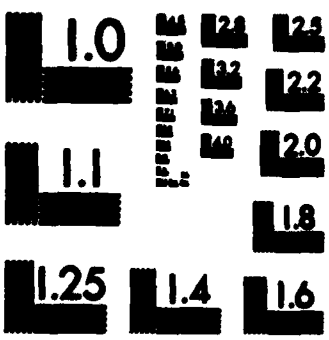

MICROCOPY RESOLUTION TEST CHART
NATIONAL BUREAU OF STANDARDS-1963-A

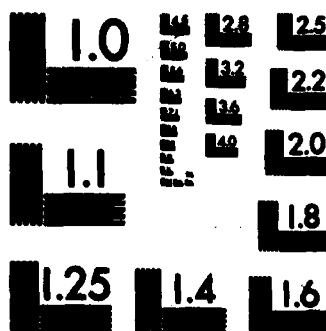

MICROCOPY RESOLUTION TEST CHART
NATIONAL BUREAU OF STANDARDS-1963-A

WASHINGTON UNIVERSITY IN ST. LOUIS

NUMERICAL ANALYSIS OF SEMICONDUCTOR DEVICES USING MICROCOMPUTERS

P.S.L. CHEN
F.J. ROSENBAUM
R.E. GOLDWASSER

Department of Electrical Engineering
Washington University
St. Louis, Mo. 63130

JULY 1982

TECHNICAL REPORT ONR-82-3

Office of Naval Research
Arlington, Va 22217

Contract: N00014 - 79 - C - 840
Contract Authority: NR SRO - 004

TABLE OF CONTENTS

LIST OF FIGURES

NUMERICAL ANALYSIS OF SEMICONDUCTOR DEVICES USING MICROCOMPUTERS

1. INTRODUCTION

The development of semiconductor electronics can be measured in terms of improvements in device switching speed, cut-off frequency, geometric dimensions and complexity. The application of new materials, advances in material preparation and quality, and the creation of new fabrication technologies have all been necessary to meet the ever increasing demands of the industry. Today, for example, Gallium arsenide (GaAs) field effect transistors (FETs) with 0.5 micron gate lengths are commonplace, and current research efforts are directed toward devices with even smaller features.

Greater device and material complexity has brought with it the need for improved analysis procedures. In many cases, closed form solutions to the often nonlinear systems of equations formulated to represent these devices are not tractable. Designers have, quite naturally,

turned to the use of computers to predict device characteristics and to gain insight into device physics. There has grown up an effort in numerical analysis and device modeling that parallels developments in the rest of the field.

The problems that this segment of the device community face include limitations placed on the size and complexity of devices that can be studied by computer memory size, machine speed, and cost of computing. Issues such as the selection of boundary conditions, the convergence of solutions, their accuracy, nonlinear optimization strategies and the like must be dealt with on a case by case basis. The cost of simulations can be prohibitive or can limit the ranges of parameters that can be considered.

The purpose of the work reported here is to develop a low cost modeling technique. The work is directed toward the use of small computers which normally have severe memory restrictions relative to the capacity of larger machines. A further goal is to employ an approach where the convergence of the solutions and their accuracy can be insured. The intention is to provide a user oriented package that can be readily reconfigured to allow for the numerical analysis of arbitrary devices. The results of these efforts are reported here.

One of the earliest uses of computers to solve a semiconductor device problem was the self-consistent

iterative scheme for one-dimensional steady-state calculation reported by Gummel (1)*. Two years later a transient numerical analysis for solving Gunn diode problems was published by McCumber and Chynoweth (2). From 1968 to 1973, many papers reported techniques for the one-dimensional analysis of a variety of devices (3-7). Among them the work of Hachtel,et. al (6) gives, perhaps, the most general and efficient analysis for junction device modeling.

For devices with comparatively simple geometries, such as bipolar transistors, one-dimensional numerical analysis might be adequate. However, modern designs involve devices so complicated that this analysis fails to offer a sufficient and accurate evaluation of device characteristics. Therefore, two-dimensional or even three-dimensional numerical analysis becomes necessary for device designers. The first two-dimensional solutions appeared in 1969, reported by Slotboom (8) and Kennedey and O'Brien (9), separately. Following these, the FET became a popular device for two-dimensional investigation (10-19). In 1976, Yamaguchi and Kodera (20) reported a sucessful treatment to reduce the computing effort by introducing a regional model.

* The number in parentheses in the text indicate references in the bibliography.

Up to this point the numerical techniques used in device simulations were based on the finite difference method. The physical model used almost universally is the well known diffusion model which includes Poisson's equation and the current continuity equation. In other words, the nature of the problem is to apply a finite difference scheme to solve the system of nonlinear partial differential equations as a boundary value problem. Seqential iteration is applied until the solution converges.

The finite element method was introduced in device modeling literature in 1974 (21-27) and now provides an alternative to the finite difference method for discretization. Reasons for using the finite element method include (1) ease in treating irregular geometries, (2) automatic conservation of current, (3) ease in local refinement of mesh size, and (4) ease in constructing higher order approximations. However, this is not to say that the finite difference method has lost its value in device modeling. Rather, with its simplicity and reliability, this method is still useful in most cases.

A common assumption made by many authors is that the device under consideration can be described by a two-dimensional model. This is generally true and the result is adequate for engineering purposes. However for those devices where the cross-section cannot be taken

uniform over the entire third dimension, three-dimensional analysis becomes a necessity. Up to the present time, this kind of treatment is rare in the literature (28). Recently, a program named FIELDAY, developed by IBM, was reported (26). This program simulates semiconductor devices of arbitrary shape in one, two or three dimensions operating under transient or steady-state conditions. Also, this program enables users to rapidly generate new models and analyze the results. It is believed to be the most general and efficient algorithm for device design purposes at the present time.

Computer storage requirements and processing costs have restricted computer-aided design activity to those institutions capable of bearing the expense. However the recent introduction of personal computers has made it feasible to do certain classes of device simulations very cost effectively. To achieve this purpose, a simulation technique must be found that fits with the comparatively small CPU memory space available for calculation. A newly developed modified decoupled method has been successful in satisfying this requirement. Based on this, a user oriented program suitable for the simulation of metal-semiconductor devices has been developed and is reported here. The approach can be applied to any semiconductor device.

In this algorithm, a five point finite difference scheme was chosen for simplicity. It can be shown that the finite element method can also be applied equally well. The Newton-Raphson iteration scheme combined with a direct matrix solution technique will always yield a converged result, especially for diagonally dominant matrix systems of the type encountered here. Of course, there are some natural limitations which dominate the accuracy of the result and the device area that can be simulated, such as the round-off error, the mesh Debye length limitation, the size of the memory available, the accuracy of boundary values, and so on.

An additional purpose of this work is to develop a new family of devices, namely the geometrically controlled metal-semiconductor diode. With the aid of the program mentioned above, two new types of diodes have been investigated.

1.1 NUMERICAL ANALYSIS (29)

The diffusion model is generally accepted in device modeling and requires no further discussion. To obtain a solution, Poission's equation, the current equation, and the continuity equation are solved together numerically, subject to the appropriate boundary conditions. In this work, for simplicity, generation and recombination processes are neglected. Likewise, the formulation is restricted to a static analysis and so the time dependent

terms are also omitted. Therefore, the continuity equation can be combined with the current equation, thereby reducing the problem statement to two equations in two unknowns; the potential and carrier concentration at each point in the device.

There are three steps used in numerical analysis: (1) discretization, (2) solution and (3) iteration. Discretization describes the process of converting a continuum problem into its discrete version (30). For this purpose, either the finite difference or finite element method can be chosen. In either case, two sets of nonlinear algebraic equations result after discretization, one from Poisson's equation, the other one from the current equation. Step two is to solve the above equation sets. Two different methods are accepted, the coupled method and the decoupled method. With the coupled method the two sets of equations are solved simultaneously. In the decoupled method they are solved serially. For iteration, either the direct iteration or the Newton-Raphson method is available. This will be discussed further in chapter 3.

The advantages and disadvantages of the finite difference and finite element methods have been metioned previously. In this work, the finite difference method has been chosen to simplify the programming work and to allow more attention to be paid to developing a new approach to

be described later. The coupled method requires approximately 4 to 9 times the amount of memory needed by the decoupled method, for unipolar and bipolar devices, respectively, and is good for strongly nonlinear types of problems. The decoupled method, which solves weakly nonlinear problems sucessfully, is the most widely used approach. Direct iteration is simple but has only a first-order rate of convergence, while the Newton-Raphson method requires a more complicated procedure but promises second-order convergence. Since numerical analysis using a minicomputer is emphasized in this work, special accomodation is needed for the limited memory space available. Considering the massive memory required by the coupled method, we have rejected it in favor of the decoupled method. However, with this method, convergence is not guaranteed.

In chapter 3, a new treatment to manipulate and solve this problem is reported, called the modified decoupled method. This method employs the Newton-Raphson technique and so it is suitable for solving weakly or strongly nonlinear problems. The results are as good as those obtained using the coupled method.

In the numerical analysis of semiconductor devices there are some additional matters to be considered. Since device simulation is, basically, the solution to a boundary value problem, the accuracy of the boundary

values used, such as carrier concentration and potential at the contacts, directly affects the accuracy of the results. Unfortunately, precise boundary conditions are not well understood yet. For example, the exact carrier concentration at a Schottky-barrier contact is not known. Therefore, contact problems need to be studied in more detail. The same argument can be applied to the assumed carrier velocity-electric field and diffusion coefficient-electric field relations which depend on the semiconductors used.

Mesh spacing is another factor which affects the accuracy of the numerical results, It will be shown in chapter 3 that, in general, the Debye length restriction is a good reference to guarantee convergence.

Once the problem has been formulated, reasonable boundary conditions defined, computer programming completed and numerical solutions obtained, one is faced with the task of verifying the validity of the results. There are three means available to the device designer to check the self-consistency of the results of the simulation.

1. Conservation of current: The current into the device should be equal to the current out of the device.
2. Comparison with the one-dimensional result: Sometimes one-dimensional results are well known analytically and/or phsically. These are good references for comparison.
3. Symmetry: With symmetrical or antisymmetrical geometries the results should conserve the corresponding symmetry properties which can be used as a reference as to the self-consistency of the solution.

1.2 APPLICATIONS IN SEMICONDUCTOR DEVICES

In this work, a two-dimensional self-consistent computer program has been written for a 64K-byte HP 9825B desktop calculator to investigate the electrical properties of devices with arbitrary contact configurations and general boundary conditions. It has been applied to two new types of devices which show promise as microwave and/or millimeter-wave, (mm-wave), devices.

GaAs, Schottky-barrier diodes (SBDs) are widely used in microwave and mm-wave applications such as detectors, mixers, limiters and multipliers. Especially for mm-wave applications, usable devices require a low noise figure, low parasitic spreading resistance and low barrier capacitance. GaAs is a material which lends itself to

meeting all these requirements (31). The one-dimensional behavior of metal-semiconductor rectifier systems, i.e. Schottky-barriers are well understood. However in many devices, such as the metal-semiconductor field effect transistor (MESFET), the contact geometries are distributed and so a two-dimensional model for the device is needed. Moreover, a model for GaAs devices must accomodate nonlinear material properties, such as field-dependent velocity and the diffusion. Although it may be possible to formulate the general problem analytically, the solution of the resultant nonlinear set of equations can best be obtained numerically.

Mixer diodes employing Schottky-barrier contacts are found to be particularly useful in high resolution radar, microwave communications, and radio astronomy. Typically their cutoff frequencies are in the range of 400 to 1000 GHz. Some of these diodes, such as beam leaded ones, can go beyond 1000 GHz (32). In most of the cases, low turn-on voltage is desired to increase detector sensitivities in some laboratory test equipment and especially in systems where local oscillator power is limited (33). Here, the turn-on voltage is defined as the applied voltage needed to obtain a particular forward current, for example 1 μA (Figure 1.1). The turn-on voltage is closely related to the barrier height of the rectifying system. For low turn-on voltage, low barrier

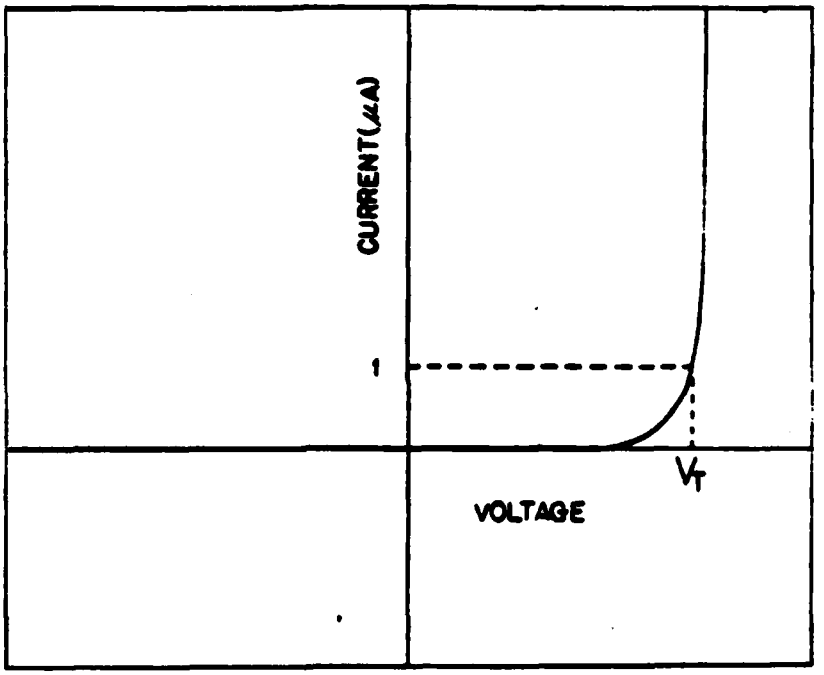

Figure 1.1 Turn-on voltage (V_T) of a Schottky-barrier mixer diode. V_T is the applied voltage corresponding to 1 μA current.

height is required. Under regular fabrication procedures, for a given Schottky metal and a particular semiconductor material, the barrier height should be a fixed value. However the number of choices for the metal is limited by technical considerations. Some barrier height lowering techniques can be applied to meet this requirement, such as high temperature processing (34), interlayer charge control using ion implantation (35), and the planar doped barrier (36).

The work presented here reports a new method to control the turn-on voltage of rectifying contacts using conventional Schottky metal barriers on arbitrary semiconductors. This new approach involves including the contact geometry as part of the design. This method has been proven to be simple, effective and can be achieved at low cost.

1.2.1. Gap Controlled Metal-Semiconductor Diode

The first device under consideration is called the Gap diode. Its current-voltage characteristic is controlled by a geometric gap between adjacent Schottky barrier regions at the blocking contact on one side of the diode. Physically, it can be expected that the effective barrier height of the Gap diode can be adjusted to any desired value between zero and the characteristic barrier height of the Schottky metal on the semiconductor material. This means that the applied voltage required to turn on the

diode is adjustable simply by changing the width of the gap. This device has been demonstrated experimentally. Striking similarity between the predicted and experimental I-V curves was observed (37).

1.2.2. Antisymmetric Metal-Semiconductor Diode

The second new device under investigation is called the Antisymmetic diode. Just as the Gap diode is a modified version of the Schottky-barrier diode, the Antisymmetric diode is a modified version of an antiparallel SBD pair. It has been shown (38) that the antiparallel SBD pair can be pumped subharmonically at one half of the local oscillator frequency and can be used as a subharmonic mixer. In microwave and mm-wave frequency applications, this has several advantages including relaxed requirements on the local oscillator frequency and power, a reduced noise figure and an improved burn-out rating. However two disadvantages of this structure are the difficulty in fabricating a completely balanced diode pair including the necessary circuit and contact, and secondly the turn-on voltage is not adjustable. The antisymmetric diode described here is one approach to solve these problems.

1.3 SCOPE OF THIS STUDY

The main purposes of this study are to develop a computer-aided analysis for two-dimensional metal-semiconductor devices, and to use it to design new types

of microwave and mm-wave devices. In Chapter 2 one-dimensional metal-semicondutor physics is reviewed with emphasis on the depletion approximation and deviations from the ideal case. Chapter 3 describes computer-aided simulation techniques for one and two dimensions. A modified decoupled method is developed for the solution of coupled nonlinear equations suitable for use on small computers. Some technical problems are discussed, such as boundary values, mesh sizes, and so on. A one-dimensional example of a Schottky-barrier junction is presented and the results compared with those of the one-dimensional depletion approximation.

The analysis method is applied to a new microwave diode called the Gap diode. Chapter 4 presents the results of the simulation and compares them to experimental results. Chapter 5 reports another new diode, the antisymmetric diode which is another potential microwave and mm-wave device. Theoretical results are presented.

2. ONE-DIMENSIONAL METAL-SEMICONDUCTOR DIODE ANALYSIS

2.1 INTRODUCTION (39)

In this chapter, the characteristics of the one-dimensional metal-semiconductor diode are discussed in order to develop a basic understanding about the diode and to provide background for two-dimensional analysis.

Metal-semiconductor contacts are also called Schottky-barrier contacts. In the area under the Schottky metal contact, there exists a region almost depleted of free carriers compared to the concentration of electrons supplied by donor atoms. An electric field exists in this depletion region supported by the fixed charge of the ionized immobile donors. The extent of the depleted region, W, under zero bias is called the depletion length.

Figure 2.1 (a) shows an n-type semiconductor diode comprising a Schottky metal contact and an ohmic contact applied to the semiconductor. The band diagram and the electron current component corresponding to forward, zero and reverse bias cases are shown in Figure 2.1 (b), (c) and (d), respectively. Here the diode length, L, (the length of the bulk region), is assumed to be greater than the depletion length, W_o. An ideal ohmic contact is defined as a thermal equilibrium contact without a potential barrier and with an infinite surface recombination velocity (40). The potential difference

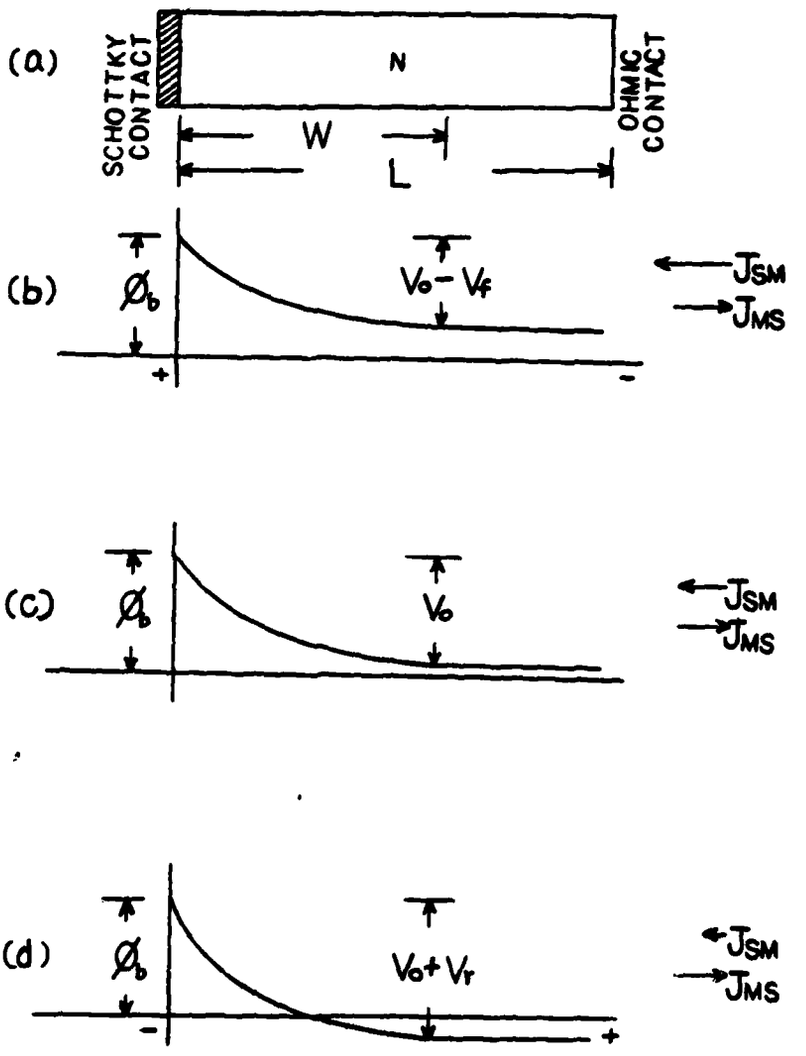

Figure 2.1 A Schottky-barrier diode band diagram and electron current density under (b) forward (c) zero (d) reverse bias conditions.

between the Schottky metal contact and the edge of the depletion region, denoted by V_o, is called the contact potential, built-in potential, or diffusion potential. In Figure 2.1, the barrier height ϕ_b is the difference between the Schottky metal work function and the electron affinity of the semiconductor. V_f and V_r are the magnitudes of the forward and reverse bias voltages, respectively. The elecron current from the semiconductor to the Schottky metal contact is denoted by J_{sm} and that from Schottky metal contact to semiconductor is denoted by J_{ms} . The barrier height as seen from the metal side stays the same over a wide range of applied voltages, V, between V_o and reverse breakdown voltage. So J_{ms} remains constant. On the other side, J_{sm} which is the current density from the semiconductor to the metal must equal J_{ms} when no bias is applied. This is shown in Figure 2.1 (c). The forward bias voltage V_f decreases the diffusion potential and allows electrons to surmount the barrier from the semiconductor to the metal, so that J_{sm} increases. The reverse bias voltage V_r increases the diffusion potential and decreases the number of electrons able to surmount the barrier from the semiconductor to the metal, so that J_{sm} decreases. For large V_r , J_{sm} will come close to zero. In this case, J_{ms} can be understood to be the saturation current density.

There are two mechanisms for charge transport over the potential barrier of Figure 2.1. If electrons have enough thermal energy to surmount the barrier then according to thermionic-emission theory (39), the total current density, J_n , is related to the applied voltage, V, by

$$J_n = A^* T^2 \exp(-qV_o/kT)[\exp(qV/kT)-1] \qquad (2.1)$$

where A^* = 120 (m^* /m) Amp $cm^{-2} \cdot K^{-2}$, for which m^* /m is the ratio of semiconductor effective mass to free electron mass. For GaAs, this ratio is 0.072 (39). The temperature is in degrees Kelvin. According to diffusion theory (39,41), the total current can be written as

$$J_n = qN_d \mu_n E_{max} \exp[-qV_o/kT)[\exp(qV/kT)-1] \qquad (2.2)$$

where q is electronic charge, N_d is the doping concentration of the bulk region, μ_n is the clectron mobility, and E_{max} is the field strength at the Schottky contact. These two completely different mechanisms predict similar results and both are accepted. In fact, it is possible to make SBDs in which the I-V curves are very close to these predictions, especially in the forward bias case (39). However, effects such as quantum-mechanical tunnelling through the barrier and hot electrons, to name a few, cause departures from the

aforementioned ideal results. This will be explained later.

In the practical case, under forward bias, the I-V curve increases exponentially as theory predicts. Usually, significant current conduction will be detected beyond the turn-on voltage which is very close to the built-in voltage. On the other hand, under reverse bias, the I-V curve of the real case is not so close to the predicted results. In fact the reverse current increases with the voltage. Eventually the avalanche breakdown process will dominate and this results in a sharply increasing current when V approaches $-V_{BD}$. This will be dissussed later. A typical I-V curve for SBD is shown in Figure 2.2.

2.2 ONE-DIMENSIONAL APPROXIMATION

The usual treatment of the metal-semiconductor junction considers a one-dimensional configuration in which the contact metal is infinite in extent. The potential distribution in the bulk semiconductor region can be calculated from Poisson's equation using a suitable approximation called the depletion approximation.

The potential and the field distribution are described in one-dimension by Poisson's equation:

$$\frac{d^2\psi}{dx^2} = \frac{q}{\varepsilon}\,(n-N_d) \qquad (2.3)$$

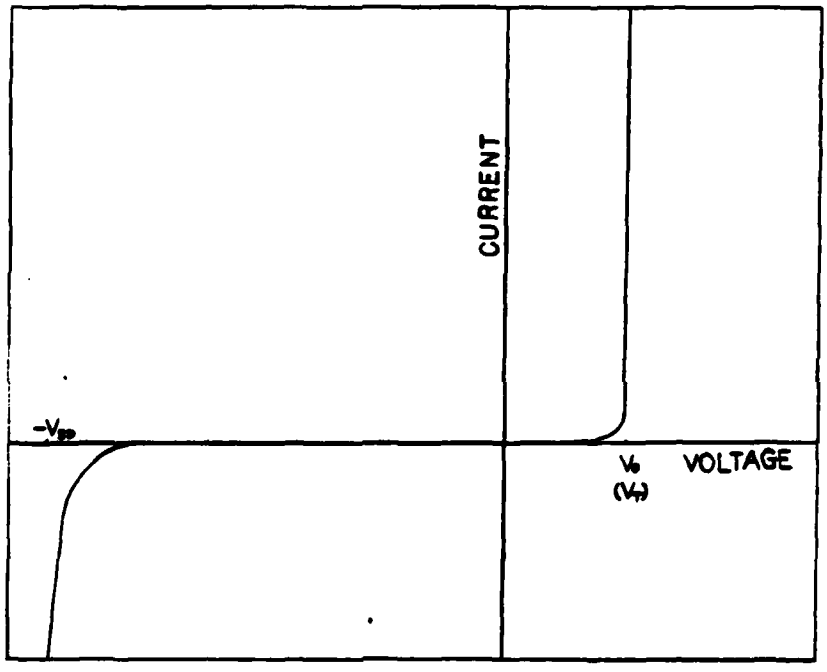

Figure 2.2 A typical I-V relation for a Schottky-barrier diode. V_o denotes the built-in voltage and V_{BD} the reverse (avalanche) breakdown voltage.

A voltage V is applied to the diode shown in Figure 2.3. If at x = 0, the potential is zero, then the potential at W will be Vo - V, due to the definition of W. Beyond the depletion edge x = W, i.e. outside the depletion region, the field is very close to zero, since here the electron density, n, is so close to N_d that the right hand side of equation 2.3 is effectively zero, and the potential is constant. Inside the depletion region, n is so small that its value can be neglected, and the field intensity increases linearly from zero at the edge of depletion region to a maximum value at the Schottky metal contact. The potential here can be described by a quadratic function of x. This is a good approximation, since for the electrons to climb the potential barrier, q (Vo - V), the value of (n - Nd) must change drastically in a very short distance around the depletion edge.

Explicitly, the boundary conditions are

Potential:

$$\psi = 0 \qquad \text{for} \qquad x = 0$$

$$\psi = V_o - V \qquad \text{for} \qquad W \leq x \leq L \tag{2.4}$$

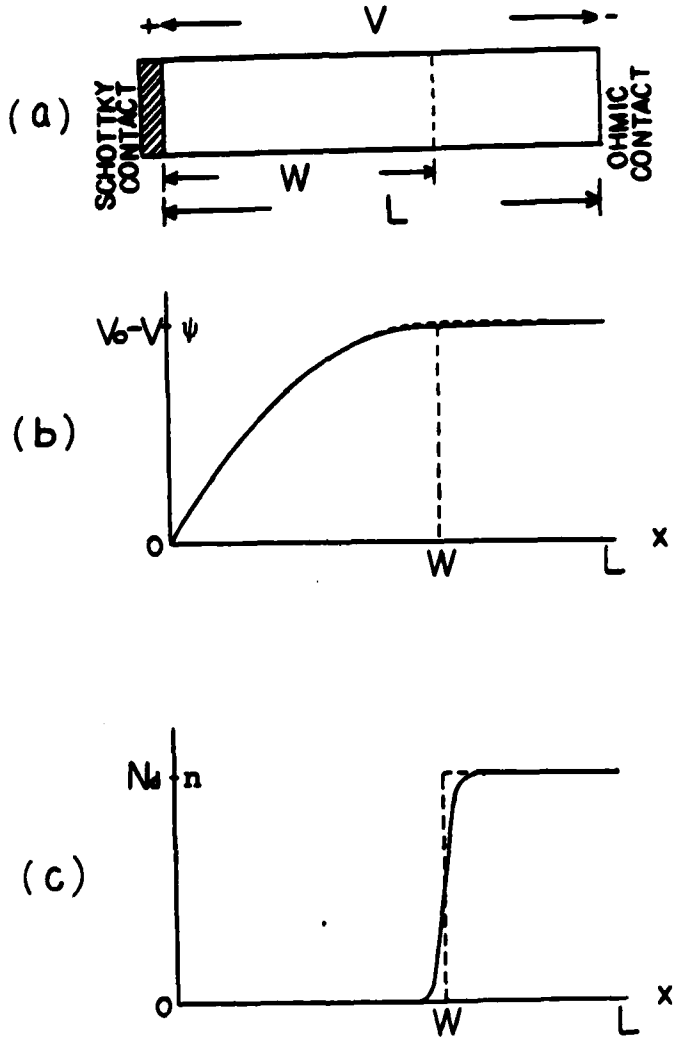

Figure 2.3 The potential distribution (b) and electron concentration (c) of an n-type Schottky-barrier diode (a). The broken lines represent the depletion approximation.

carrier concentration :

$$n = 0 \qquad \text{for} \qquad 0 \leq x \leq W$$

$$n = N_d \qquad \text{for} \qquad W < x \leq L$$

Inside and outside the depleted region equation 2.3 becomes:

$$\frac{d^2\psi}{dx^2} = \begin{cases} -\frac{q}{\varepsilon} N_d & 0 \leq x \leq W \\ 0 & W < x \leq L \end{cases} \tag{2.5}$$

Using the following relation as a boundary condition

$$\frac{d\psi}{dx} = 0 \qquad W \leq x \leq L \tag{2.6}$$

yields

$$\frac{d\psi}{dx} = -\frac{q}{\varepsilon} N_d (x-W) \qquad 0 \leq x \leq W \tag{2.7}$$

and so

$$\psi(x) = -\frac{q}{\varepsilon} N_d \left(\frac{1}{2} x^2 - Wx\right) \qquad 0 \leq x \leq W \tag{2.8}$$

In order to satisfy the boundary condition at x = W, the value of W should be

$$W = \left[\frac{2\varepsilon(V_o - V)}{q\,N_d}\right]^{1/2} \tag{2.9}$$

Equation 2.7 shows that the field strength, $E = -\,d\psi / dx$, at x = 0, i.e. the surface of semiconductor, is maximum,

$$E_{max} = \frac{q}{\varepsilon} N_d W = \left[\frac{2qN_d(V_o - V)}{\varepsilon}\right]^{1/2} = \frac{2(V_o - V)}{W} \tag{2.10}$$

and decreases linearly in x to a minimum value zero at x = W. The direction of the field is from the semiconductor to the metal. The total charge in the depletion region is

$$Q = \varepsilon\, E_{max} A = qN_d WA \tag{2.11}$$

and the junction capacitance is

$$C = \left|\frac{dQ}{dV}\right| = \frac{\varepsilon}{W} A \tag{2.12}$$

where A is the diode area.

2.3 CURRENT-VOLTAGE MODEL

As mentioned previously, there are two approaches to describe the I-V relation of a Schottky diode, i.e. the thermionic-emission and the diffusion model. Since the

diffusion model can be generalized and applied to a two-dimensional structure, a detailed study of it is worthwhile. The thermionic-emission model is omitted here.

The expression for current in terms of drift and diffusion components is

$$J_n = qn\mu_n E + qD_n \frac{dn}{dx} \tag{2.13}$$

where positive J means in the positive x direction, D. is the diffusion coefficient for electrons and is taken independent of position. The problem is to find an expression for Jn in terms of the applied voltage V. Before starting to calculate the current, it should be noted that the diffusion model is based on the following assumptions:

1. The current through the barrier is due to the combined effects of drift and diffusion in the depletion region.
2. The barrier height is much greater than kT/q.
3. The carrier concentrations at x = 0 and W are unaffected by the forward bias voltage.

The simplest expression relating D_n and μn is the Einstein relationship.

Since the static case is assumed, $dJ_n/dx = 0$, and J_n is a constant. Rewriting equation 2.13 by adding a factor $\exp(-q\psi/kt)$, together with equation 2.14, gives

$$J_n \exp(-q\psi/kT) = D_n \frac{d}{dx} [n \exp(-q\psi/kT) \qquad (2.15)$$

When V = 0, there is no current ($J_n = 0$). At x = W, the potential is the built-in value, = Vo and $n = N_d$; at x = 0, $\psi = 0$, and n = n(0). So from equation 2.15 one obtains,

$$n(0) = N_d \exp(-qV_o/kT) \qquad (2.16)$$

From assumption 3, equation 2.16 will be applied in all cases. With the aid of equations 2.8, 2.9, 2.10, and integrating with respect to x from 0 to W, yields equation 2.2.

2.4 EXACT ANALYSIS

Instead of the depletion approximation, sometimes an exact analysis is desired, especially for the two-dimensional case. The charge density and potential are related by Poisson's equation. See equation 2.3. The current density, in terms of drift and diffusion, is described in equation 2.13. If the Einstein relationship is assumed, a simple expression for the field at the contact, i.e. E_{max} , can be found.

If $J_n \approx 0$, such as is obtained for a bias voltage less than the turn-on voltage, or in reverse bias, equation 2.13 can be rewritten as

$$\frac{d}{dx}\left[n \exp(-q\psi/kT)\right] \approx 0 \qquad (2.17)$$

Integrating and applying the boundary condition at $x = L$, $n = N_\alpha$, where the potential is $V_o - V$, one obtains

$$N_{(x)} \approx N_d \exp\left[-\frac{q}{kT}(-\psi+V_o-V)\right] \qquad (2.18)$$

Substituting $n(x)$ in Poisson's equation, one obtains, after some manipulation,

$$\frac{d}{dx}\left(\frac{d\psi}{dx}\right)^2 \approx \frac{2qN_d}{\varepsilon}\left\{\exp\left[\frac{q}{kT}(\psi-V_o+V)\right]-1\right\}\frac{d\psi}{dx} \qquad (2.19)$$

Integrate this equation from $x = 0$ to L to get

$$\left(\frac{d\psi}{dx}\right)^2_{x=0} - \left(\frac{d\psi}{dx}\right)^2_{x=L} \approx \frac{2qN_d}{\varepsilon}\left(-\frac{kT}{q} - V + V_o\right) \qquad (2.20)$$

For a Schottky diode in which the length of the semiconductor is much greater than the depletion length, i.e. $L >> W_o$,

$$\left.\frac{d\psi}{dx}\right|_{x=L} \approx 0 \qquad (2.21)$$

the value of E_{max} will be

$$E_{max} = \left|\frac{d\psi}{dx}\right|_{x=0} \approx \left[\frac{2qN_d}{\epsilon}\ (V_o - v - \frac{kT}{q})\right]^{1/2} \qquad (2.22)$$

Comparing this with the expression for E_{max} derived from the depletion approximation, equation 2.10, the only difference is the term kT/q. However, from assumption 2, $kT/q << Vo$, so E_{max} in both cases is identical, when equation 2.21 holds.

Even in the one-dimensional case, closed form solutions for n and ψ are not attainable, because of the nonlinear nature of equation 2.19. On the other hand the depletion approximation is accurate enough for most practical purposes. For the potential, the difference in results is negligible; for the electron charge concentration, however, the exact n(x) is a smoothly varying function that rises from 10 % of N_d to 90 % around the depletion edge x = W, rather than jumping discontinuously from 0 to N_d at x = W for the depletion approximation. The corresponding potential change is less than 2kT/q. Also the electron concentration at x = W is about 50 % of Nd in the exact case. (See Figure 2.3, and for further detail see Chapter 3 for a one-dimensional simulation)

2.5 PRACTICAL METAL-SEMICONDUCTOR DIODE

The Schottky diode discussed above is an ideal one. In this section several practical departures from ideality are discussed.

2.5.1 Image Force

When an electron moves from the semiconductor to the Schottky metal, an image force exists which affects the electron motion. This force lowers the potential barrier by an amount (39,40)

$$\Delta\phi_b = 2x_m E_{max} \tag{2.23}$$

$$x_m = \left[\frac{q}{16\pi\epsilon E_{max}}\right]^{1/2} \tag{2.24}$$

where x_m is the distance to the peak of the barrier from the Schottky contact. If the doping concentration is $N_d = 10^{17}cm^{-3}$, then under zero bias E_{max} is of the order of 10^6 V/cm, x_m is of the order of 10 A°, and $\Delta\phi_b$ is less than 0.05 volt. This estimation suggests that the image force effect can be neglected in diode simulations if the doping concentration is not too high.

2.5.2 Ideality Factor

The current-voltage relationships described by equations 2.1 and 2.2 are for the ideal case. In practice, no I-V characteristics exactly obeying these equations have been observed. An ideality factor n is usually included in the I-V relation to match the theory to experimental results.

$$J_n = J_o \exp(-qV_o/kT) \exp(qV/nkT) [1-\exp(-qV/kT)] \quad (2.25)$$

where Jo is $A^* T^2$ or $qN_d\mu_n E_{max}$, and usually $1 < n < 1.2$. There are several means by which to explain the factor n added here, including a voltage dependent barrier height, interfacial layer effects, temperature effects and so forth. (For further information see (39))

2.5.3 Tunnelling

In reverse bias, if the potential barrier becomes thin enough, significant tunnelling of electrons from the metal to the semiconductor might take place. Also at high doping concentrations, say of the order of 10^{19} cm^{-3} or more, this phenomenon might be observed. In this work, since comparatively low doping concentrations are used and high reverse bias cases are not of interest, the tunnelling effect is neglected in the simulations. For reference, see (39).

2.5.4 Interfacial Layer

In the manufacturing of SBDs it is not easy to remove the thin oxide layer often present between the metal and the semiconductor. Such an interfacial layer lowers the barrier height and gives some series resistance to the current, so that the I-V relationship departs from the ideal case. Thus the ideality factor will change also. Since the thickness of the interfacial layer might be of the order of 10 A°, to simplify the simulations in two-dimensional structure, this possibility is omitted.

2.5.5 Reverse Characteristics

According to thermionic-emission theory (39), in reverse bias, the current saturates at a constant value

$$J_{sat} = A^{*}T^{2} \exp(-qV_{o}/kT) \qquad (2.26)$$

However in the real case, such an ideal phenomenon is not seen. In fact, the current increases gradually with voltage. There are several reasons which contribute to this, including the voltage dependency of the barrier height, the effect of tunnelling, the edge effect, the image force, the carrier generation in the depletion region, and so forth. Although the diffusion theory predicts an increasing reverse current, it needs some modification to achieve a closer prediction to experimental results.

When a high reverse bias voltage is applied, the reverse current may grow rapidly. This sort of breakdown phonomenon can result from two different mechanisms. The first one is called Zener breakdown, which operates at lower voltages; The second one is called avalanche breakdown, which operates at higher voltages, beyond the Zener breakdown. Zener breakdown can be thought of as a "soft breakdown" which is due to field ionization and tunnelling. Usually such a breakdown phenomenon occurs in those diodes with heavy doping and under low reverse bias voltages. The typical electric field is of the order of 10^6 V/cm. (39,42) The avalanche breakdown mechanism involves carrier ionization and multiplication with high reverse bias voltages. (39,42)

2.5.6 Field Dependent Electron Velocity And Diffision Coefficient - Hot Electron Effects

In equation 2.13 the current is divided into two terms. The first is the drift current $qn\mu_n E$, where $\mu_n E$ is the electron velocity V_n :

$$V_n = \mu_n E \tag{2.27}$$

The second term is the diffusion current $qD_n dn/dx$.

In GaAs, under high fields, the electron velocity, Vn, is a nonlinear function of the field (43). According to Thim (44), an analytic approximation for the

velocity-field relationship is

$$V_n = [\mu_n E + V_s (\frac{E}{E_o})^4]/[1 + (\frac{E}{E_o})^4] \qquad (2.28)$$

where Vs is the saturation velocity, Eo is the threshold field. Here the temperature dependent relation has been omitted and room temperature is assumed. For further detail see (43). When the field is low, equation 2.28 reduces to equation 2.27. At very high fields, the velocity saturates at a value Vs.

Diffusion in GaAs does not obey the usual Einstein relation. However it is possible to modify it by including an effective energy relaxation time in the diffusion coefficient (45).

$$D_n(E) = \frac{kT}{q} \frac{V_n(E)}{E} + \frac{2}{3} \tau_e V_n^2(E) \qquad (2.29)$$

Here τ_e is the energy relaxation time, of the order of 10^{-13} sec. for GaAs. When the field is low, the second term on the right hand side is negligible and equation 2.29 becomes the Einstein relation.

For small devices whose active region length is less than one micron, electron transport behavior is different from the discussion above. Since relaxation time processes for energy, charge and momentum are comparable with the transit time, the velocity never saturates, but

rather increases with the field (46). Generally speaking, the velocity is a function of position, time and the properties of the external load, as well as the field. The diffusion coefficient might have a similar problem. Hot electron effects have to be taken into account in the simulations presented here to achieve a result closer to reality.

With this as background, we turn now to developing the numerical techniques needed to solve the transport equations.

3. COMPUTER-AIDED DEVICE SIMULATION

This chapter describes computer-aided semiconductor device simulation techniques and presents a modified decoupled solution method using a microcomputer. The one-dimensional case is studied first. The results are evaluated and then the method is extended to two-dimensional configurations.

3.1 PHYSICAL MODEL

For simplicity, an n-doped majority carrier device is assumed, such as a MESFET, Schottky diode, etc.. The characteristics are dominated by Poisson's equations and the electron current equation:

$$\nabla^2\psi = \frac{q}{\varepsilon}(n-N_d) \tag{3.1}$$

$$\vec{J}_n/q = n\vec{v}_n + D_n\nabla n \tag{3.2}$$

all of the quantities were defined in the previous chapter. For the one-dimensional case equations 3.1 and 3.2 are the same as equations 2.3 and 2.13. In this study only one and two-dimensional behavior are considered. In the two-dimensional case, the parameters $\vec{J}_n$, ∇n and $\vec{V}_n$ are vectors having components along the x and y directions; $\nabla^2\psi$ can also be written as

$$\nabla^2\psi = \frac{\partial^2\psi}{\partial x^2} + \frac{\partial^2\psi}{\partial y^2} \tag{3.3}$$

The static current constraint

$$\nabla\cdot\vec{J}_n = 0 \tag{3.4}$$

is also needed to solve the system. As a matter of fact, equation 3.2 can be combined with equation 3.4 to remove the unknown current $\vec{J}_n$:

$$0 = \nabla\cdot(n\vec{v}_n + D_n\nabla n) \tag{3.5}$$

At the contacts and the edges of the device, the boundary values must be specified as mentioned in Chapter 2.

3.2 NUMERICAL METHODS

The finite difference method was the first to be used in device simulations. Five point formulas using rectangular meshes give the famous centered difference approximation. In order to solve the resultant system of equations efficiently, variable mesh sizes are considered. This has been discussed by Adler (47). In many devices, two- dimensional behavior is restricted only to a small part of the device. By separating the entire device into appropriate portions depending on their behavior, and defining suitable grid patterns, much computer memory and

computation time can be saved. In Adler's paper, a method which allows terminating mesh lines in finite difference simulation was reported. This idea is close to the spirit of the finite element method.

Linear piecewise polynomial functions applied on triangular meshes provide the simplest type of finite element formulation. For more accurate results, the hermite bicubic function method is a better choice (24). However this method needs more boundary conditions and more computer memory than the finite difference approach and might not be appropriate for small computer simulations. In fact, the finite element method takes more effort in programming than does the finite difference method. If the geometry is not too complicated and a degree of approximation can be tolerated, the finite difference method should be adquate for the purpose of semiconductor device modeling.

3.2.1 Techniques Of Simulation - Modified Decoupled Method

As mentioned before, the finite difference method has been elected for simulation. The first step is to discretize the device by generating mesh lines over the entire active region under consideration. An example is shown in Figure 3.1, in which the node numbering system is also included. Mesh lines can be either uniform or nonuniform depending on physical and geometrical considerations. The numbering system specifies the

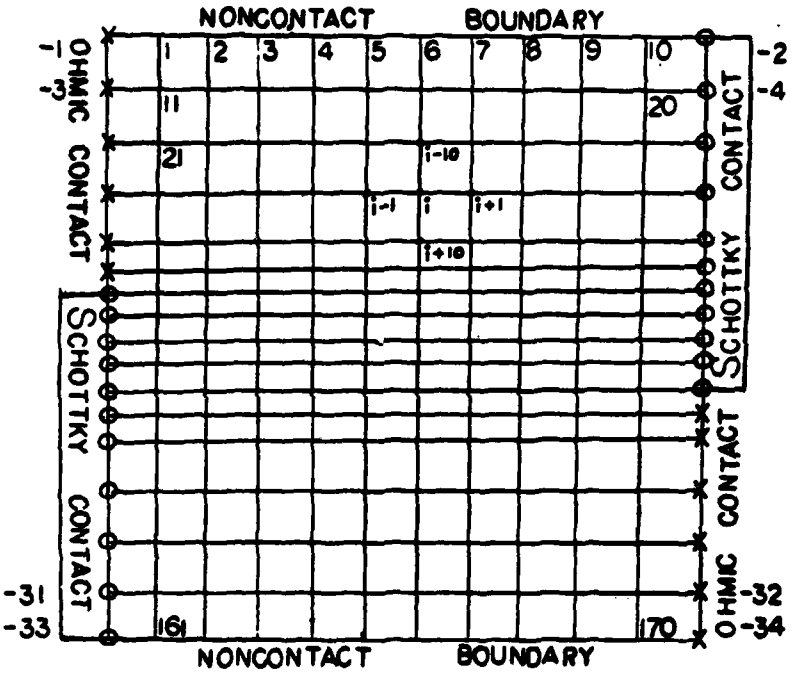

Figure 3.1 A sample configuration to show mesh lines and the node numbering system.

boundary nodes in negative numbers and the nodes inside the semicoductor in positive numbers. Values of the variables at the boundary nodes, such as those on ohmic and Schottky contacts, must be specified. At noncontact boundaries, the normal components of the current and electric field strength are all equal to zero. However, nodes on those surfaces are positively numbered and must be taken into account in calculation because there are unknown variables there as well as at the nodes inside the semiconductor. Surface charge density can also be used as a boundary condition on noncontact boundaries.

For each positive node i, Poisson's equation has a corresponding discrete version. For example : in Figure 3.1, if the adjacent nodes of i are i+1, i-1, i+10 and i-10 and all are equi-distant to i, then can be represented by

$$\frac{1}{d^2}\,(V_{i+1}+V_{i-1}-2V_i) + \frac{1}{d^2}\,(V_{i+10}+V_{i-10}-2V_i)$$

and n simply by N_i. Here V_i and N_i are the space-charge potential and electron mobile charge concentration at node i, respectively. Therefore, for each node i, there is a discrete expression for Poisson's equation with 6 node variables: 5 for potential and 1 for charge concentration. This is valid for most of the nodes inside the semiconductor. For those nodes next to the contact,

however, one of the node potential variables is known, so the total number of variables is 5. Obviously, each node on a noncontact boundary has fewer variables than those inside the semiconductor. Similarly for each node i, a discrete current continuity equation (equation 3.5) can be derived.

With suitable manipulation, the entire family of Poisson's equations, after discretization, can be expressed in matrix form as equation 3.6 and the current continuity equation as equation 3.7. Note that the total number of equations resulting from the discretization of equation 3.6 and 3.7 is equal to the total number of nodes inside semiconductor. For example, the number is 170 in Figure 3.1.

$$A\,\bar{V} = B\,\bar{N} + \bar{C}$$

$$P_{(\bar{V})}\,\bar{N} = \bar{Q}$$

Here $\bar{V}$ is a column vector $[V_1,.....,V_\ell]^t$ representing the potential at each node and $\bar{N} = [N_1,.....,N_\ell]^t$ is the electron concentration at each node. The integer ℓ represents the total number of nodes inside the semiconductor. A, B are ℓ x ℓ constant matrices, $\bar{C}$, $\bar{Q}$ are constant ℓ-column vectors, P is an ℓ x ℓ matrix and a function of potential. Note that the current $\vec{J}_n$ has

been removed by equation 3.4. Now the variables are $\bar{V}$ and $\bar{N}$. But instead of solving for $\bar{V}$ and $\bar{N}$ simultaneously, in equation 3.6, $\bar{V}$ is treated as an independent variable, and $\bar{N}$ as a dependent variable with respect to $\bar{V}$, so, as a matter of fact, equation 3.6 is solved in every iteration loop with equation 3.7 as an auxiliary function.

The Newton-Raphson method (30) starts from a truncated Taylor's expression. Concentrating on equation 3.6, after some manipulation it becomes:

$$(A\bar{V}^{i+1}-B\bar{N}^{i+1}-\bar{C}) \simeq (A\bar{V}^{i}-B\bar{N}^{i}-\bar{C}) + \left\{A-B\left[\frac{d\bar{N}}{d\bar{V}}\right]^{i}\right\} \Delta\bar{V}^{i} \quad 0 \tag{3.8}$$

$$\bar{V}^{i+1} = \bar{V}^{i} + \Delta\bar{V}^{i} \tag{3.9}$$

where i = 1, 2, 3, ... represents the index of iterations. The quantity $[\frac{d\bar{N}}{d\bar{V}}]$ is an ℓ x ℓ tangential matrix or Jacobian matrix (30) :

$$\begin{bmatrix} \frac{\partial N_1}{\partial V_1} & \cdots\cdots & \frac{\partial N_1}{\partial V_\ell} \\ \vdots & \cdots\cdots & \vdots \\ \vdots & \cdots\cdots & \vdots \\ \vdots & \cdots\cdots & \vdots \\ \frac{\partial N_\ell}{\partial V_1} & \cdots\cdots & \frac{\partial N_\ell}{\partial V_\ell} \end{bmatrix}$$

$\Delta\bar{V}^i$ can be evaluated from equation 3.8 with the result

$$\Delta\bar{V}^i = -\left\{A-B\left[\frac{d\bar{N}}{d\bar{V}}\right]^i\right\}^{-1}\left(A\bar{V}^i-B\bar{N}^i-\bar{C}\right) \tag{3.10}$$

In the above equation two terms are still unknown, that is

$$\left[\frac{d\bar{N}}{d\bar{V}}\right]^i \qquad \text{and} \qquad \bar{N}^i$$

These values can be found from equation 3.7:

$$\bar{N} = \left[P_{(\bar{V})}\right]^{-1}\bar{Q} \tag{3.11}$$

and also by differentiating it with respect to V,

$$\left[\frac{d}{d\bar{V}}\left(P_{(\bar{V})}\bar{N}\right)\right] = 0 \tag{3.12}$$

The left hand side of equation 3.12 can be separated into two terms,

$$P_{(\bar{V})}\left[\frac{d\bar{N}}{d\bar{V}}\right] + \left[\gamma_{jk}\right]_{j,k=1}^{\ell} = 0 \tag{3.13}$$

where $\gamma_{jk} = \sum_{m=1}^{\ell}\left(\frac{\partial h_{jm}}{\partial v}\, n_m\right)$; h_{jm}, v_k and n_m

are elements of $P_{(\bar{V})}$, $\bar{V}$ and $\bar{N}$ respectively. Equation 3.13 may be rearranged to read:

$$[\frac{d\bar{N}}{d\bar{V}}] = - [P_{(\bar{V})}]^{-1} [\gamma_{jk}]_{j,k=1}^{\ell} \qquad (3.14)$$

This completes the evaluation of $\Delta\bar{V}^i$ for equation 3.10. From equation 3.9, $\bar{V}^{i+1}$ can be calculated and equations 3.9 and 3.10 are ready for next iteration loop i+1.

To start the calculation, the initial $\bar{V}$ value is arbitrarily given, say $\bar{V} = \bar{V}^0 = [0,.....,0]^t$. From equation 3.7, $\bar{N}$ can be obtained, say $\bar{N}^0$, which is used in the right hand side of equation 3.6. Then equation 3.6 can be solved directly in terms of $\bar{V}$. This $\bar{V}$ is used as $\bar{V}^1$ and the aforementioned iteration procedure starts. Usually it takes 3 to 6 iterations to obtain a converged solution for $\bar{V}$. The solution of $\bar{N}$ follows through equation 3.11.

The numerical approach described above can be summarized as follows : Eliminate $\bar{N}$ in equation 3.6 by equation 3.11 and obtain

$$A\bar{V} = B[P_{(\bar{V})}]^{-1} \bar{Q} + \bar{C} \qquad (3.15)$$

This is a system of equations with variable $\bar{V}$ only. Theoretically it is possible to solve such nonlinear system using the Newton-Raphson method directly. However,

difficulties arise from manipulation of the inverse term on the right hand side of equation 3.15. This explains why it takes so many steps to process.

From the description above it is evident that the largest memory space occupied by one term is an ℓ x ℓ matrix storage. Since there is only one such matrix needed for processing at any one time, all of those terms not in use can be stored on disk. For manipulation of equation 3.14, there are two ℓ x ℓ matrix multiplications. Since each matrix may occupy more than 85 % of total CPU memory space, one of them should be stored on the disc, and the matrix operation done column by column.

3.3 COMMENTS

In this section some practical considerations about this simulation are disscussed.

3.3.1 Boundary Conditions

It is necessary to consider the boundary conditions when the simulation is carried out. At ohmic contacts, usually the ideal case is assumed, i.e. the carrier concentration is equal to the doping concentration of the adjacent semiconductor. At the Schottky contacts, in the forward bias case the carrier concentration is assumed to be given by equation 2.16. In reverse bias, at the Schottky contacts, since the effective built-in potential becomes $V_o + V_r$ the following expression is more suitable

$$n = N_d \exp\left[-\frac{q}{kT}(V_o+V_r)\right] \qquad (3.16)$$

Here, V_r is the magnitude of the reverse bias voltage. Also at the edges of the device, it is assumed that the first order partial derivatives of both carrier concentration and space-charge potential in the normal direction are zero.

3.3.2 Current Continuity Equation

For static simulations, the unknown current is eliminated by combining equations 3.2 and 3.4 to obtain equation 3.5. This makes the equation a second order partial differential equation as well as a Poisson's equation. So, in fact, two sets of boundary values are required for simulations.

If the maximum field everywhere in the device is low, the Einstein relationship holds, and the simulation is straightforward. If, however, the field is high enough to drive carriers into the nonlinear parts of the velocity-field curve and the diffusion-field curve for a significant part of the carrier's trajectory, (in case of GaAs, see section 2.4.6), there are two choices:

1. Equations 2.16 and 3.16 are still used, due to lack of better boundary conditions available.
2. Solve Poisson's equation and the continuity equation numerically, in one dimension, taking hot electron effects and the value of the current, i.e. equation 2.2, into account, to obtain the carrier concentration at the Schottky contact for each applied voltage.

The first choice is simple but, in two-dimensional simulations, the total current calculated would be unreasonable under certain conditions. However, in two-dimensional simulation of MESFETs for example, usually the metal gate is reverse biased, and negligible current is carried by the gate. So equation 3.16 and zero current density are both assumed without loss of generality (20). The second choice might be good for fine meshes, However, the memory capacity of the small computer used here limits the smallest mesh size, and so in some cases unreasonable carrier concentrations at the Schottky contact are obtained.

3.3.3 Program And Flow Chart

Since one wants to reserve most of the computer memory for matrix operations, the program is separated into several subprograms. All the data not in use are stored on disk. Some matrix variables and array variables can represent different items at different times to minimize

the number of variables required. Caution must be exercised in programming equation 3.10, especially in calculating the Jacobian matrix as in equation 3.14, to prevent some error in differentiating each element.

Information regarding each node or element is stored on the disk, including the adjacent node or element number, the distance between each of the nodes and some identification to distinguish between nodes inside the active region and those on the boundary. The boundary values can be adjusted automatically in the main program for each applied bias. So the program can be used to simulate different structures if the input information is properly assigned.

To start the simulation, the value of the space charge potential at each node is assumed under the zero bias condition. Since the current is zero in this case, one can solve for the carrier concentration from current continuity and carry out an iteration procedure until it converges. Usually for a simulation containing 80 nodes, three to six iteration loops are common and it takes approximately 1.5 to 2.5 hours to obtain the results for one bias point on the device I-V curve, using an HP 9825B.

The flow chart for the process is shown in Figure 3.2 and a sample program is given in the appendix. Figure 3.3 shows the steps needed to operate the program. An illustration of the device configuration with mesh lines,

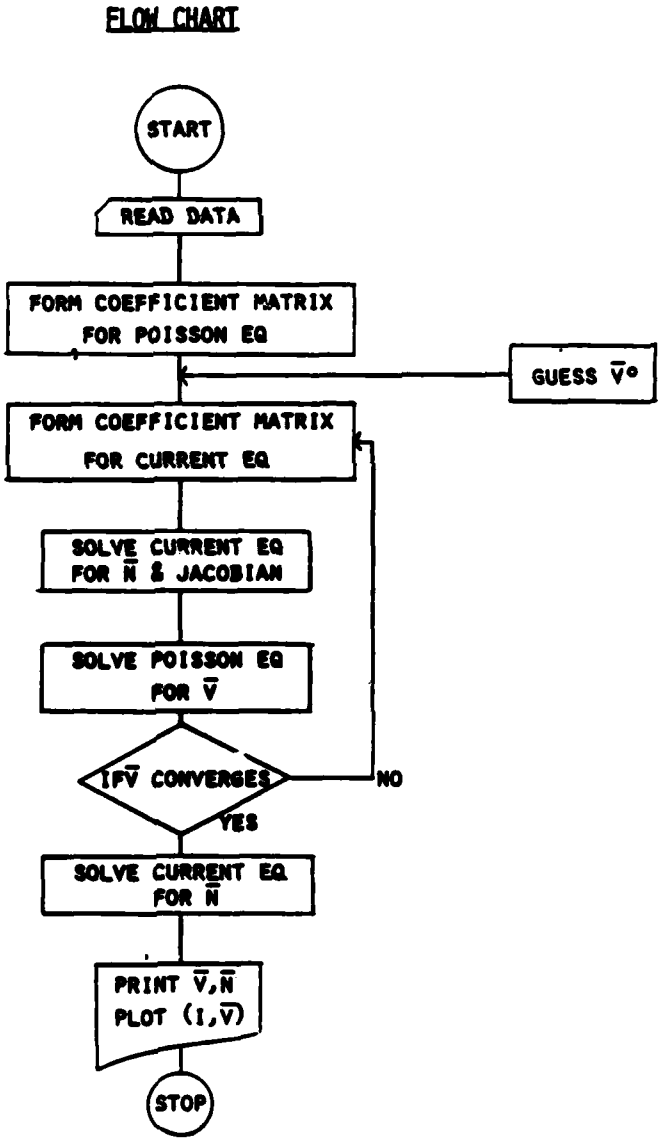

Figure 3.2 Flow chart for the computer simulation.

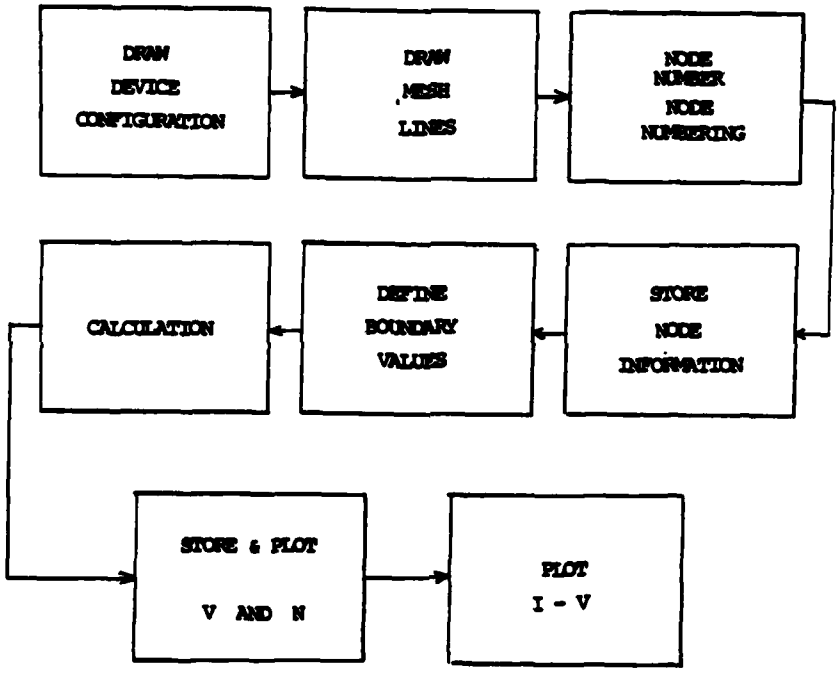

Figure 3.3 Flow diagram for simulation procedures.

and the nodes numbered is shown in Figure 3.1. To store node information, the first program in the appendix can be used as an example. Boundary values can be defined in the main program such that after the information for each node is read in, its boundary value will be given automatically before the calculation proceeds, as shown in lines 17-28 of Program 3 in the appendix. The final results of $\bar{V}$ and $\bar{N}$ for each applied bias should be stored on disk and also printed out in the same form as node numbering configuration. A typical program for this is shown by Program 7 in the appendix. Finally the I-V curve can be plotted. In the next section, considerations needed to set mesh sizes are discussed.

3.3.4 Mesh Spacing

In semiconductor device simulations, it is recommended to restrict the mesh spacing, h, to be no more than the Debye length:

$$L_{Debye} = \left(\frac{2\varepsilon kT}{q^2 N_d}\right)^{1/2} \tag{3.17}$$

i.e.

$$L_{Debye} \geq [(dx)^2 + (dy)^2]^{1/2} = h \tag{3.18}$$

where dx and dy are the mesh spacing components in the x and y directions, respectively. If this limitation is

ignored, the solutions may represent physically meaningless results (24). This restriction is mainly for those cases where the Einstein relationship holds or at least for deviations not far from it. If some nonlinear velocity-field and/or diffusion-field curves are used, the maximum spacing might be modified as (24)

$$h \simeq \frac{\mu \Delta V}{V_{sat}} < \frac{2D}{V_{sat}} \tag{3.19}$$

where V_{sat} is the saturation velocity, and ΔV is the potential change between two adjacent nodes. Also, from the discussion above, since the maximum spacing is limited, the maximum device area which we can model is also limited because of the computer memory size.

As an example to obtain some understanding about the minimum spacing, consider the conventional SBD of Figure 2.3. Under zero bias, from equation 2.18, Poisson's equation becomes

$$\frac{d^2\psi}{dx^2} = \frac{q}{\epsilon} N_d \left\{ \exp\left[\frac{q}{kT}(\psi - V_o)\right] - 1 \right\} \tag{3.20}$$

At any point x located in the area between the depletion edge W and the end of the epi-layer L, ψ is very close to Vo. Using Taylor's expansion in equation 3.20 yields

$$\frac{d^2\psi}{dx^2} \simeq \frac{q}{\varepsilon} N_d \frac{q}{kT} (\psi - V_o) \tag{3.21}$$

Let $\xi = \psi - V_o$, so equation 3.20 can be rewritten as

$$\frac{d^2\xi}{dx^2} \simeq \frac{q}{\varepsilon} N_d \frac{q}{kT} \xi \tag{3.22}$$

If the Newton-Raphson method is used, the truncation error is

$$\frac{1}{2} h^2 \frac{d^2\xi}{dx^2}$$

Assuming the mesh spacing h is no less than the Debye length, then

$$\frac{1}{2} h^2 \frac{d^2\xi}{dx^2} \geq \frac{1}{2} L_{Debye}^2 \frac{q}{\varepsilon} N_d \frac{q}{kT} \xi \tag{3.23}$$
$$= \xi$$

In other words, the error could be larger than 100 %. For two or three- dimensional structures, similar results can be expected.

The argument given above for minimum spacing is no longer valid inside the depletion region, since in this case equation 3.20 becomes

$$\frac{d^2\psi}{dx^2} \simeq - \frac{q}{\varepsilon} N_d \tag{3.24}$$

instead of equation 3.21. It can be shown that the truncation error is -kT/q, which is comparatively small compared with the potential value ψ corresponding to it. Therefore, wider spacing is allowed inside the depletion region than outside it. In general, the Debye length is a good measure for the mesh spacing. Caution should be exercised when the mesh spacing is chosen to be larger than Debye length.

If the Einstein relationship is not applied, then suitable mesh spacing related to the current equation should also be considered. Equation 3.19 is, in general, a basic criterion for that. Generally, if the mesh spacing is taken to satisfy both equations 3.18 and 3.19, reasonable results should be expected. From simulation cost considerations, it is possible to relax the spacing criterion in the interior a certain amount, but keeping a finer mesh spacing on the boundaries.

3.4 ONE-DIMENSIONAL SIMULATION

Since the conventional Schottky diode is reasonably well understood, it can be used for comparison with the one-dimensional simulation results. If they are similar, then some confidence can be placed on the results of the two-dimensional simulations. In this section we will consider only one-dimensional cases and examine the details of the static solution in a conventional GaAs SBD. The results shown in Figure 3.4 show the effect of varying

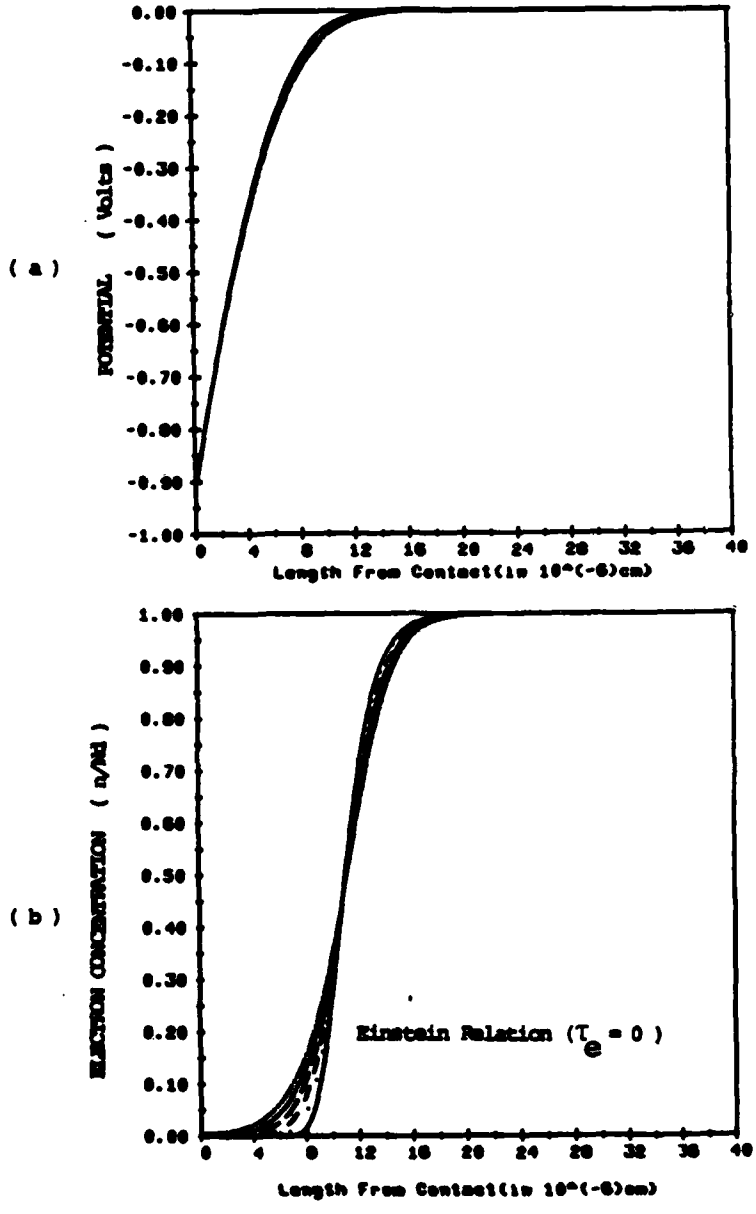

Figure 3.4 Typical results for a conventional Schottky-barrier diode. (a) potential (b) carrier concentration with $N_d = 10^{17}$ cm^{-3}, barrier height = 0.9 V, $\mu_n = 6875$ cm^{2}V^{-1}sec^{-1}, V_s = 1.1×10^7cm/sec, E_o = 3.2 KV/cm, Starting from the solid line (Einstein relation) τ_e = 0, 1, 3, 5, 7, 9 x 10^{-13}sec, depletion length = 0.11 μm.

the energy relaxation time. From this graph and the results, one observes that:

1. For a fixed bias voltage, the field strength at the Schottky contact is approximately a constant, no matter what kind of field dependent velocity and diffusion relationships are taken. Recall that

$$E = -\frac{d\psi}{dx}$$

This result can be understood as follows: From equation 2.3,

$$\left(\frac{d\psi}{dx}\right)_L^2 - \left(\frac{d\psi}{dx}\right)_o^2 = \int_o^L 2\,\frac{q}{\varepsilon}\,(n-N_d)\,\frac{d\psi}{dx} \qquad (3.25)$$

Assuming the diode length L is greater than the depletion length W, then

$$\left(\frac{d\psi}{dx}\right)_L \approx 0 \qquad (3.26)$$

Also, n is negligible inside the depletion region. Hence

$$\left(\frac{d\psi}{dx}\right)_o \approx \left[\frac{2q}{\varepsilon}\,N_d(V_o-V)\right]^{1/2} \qquad (3.27)$$

where the right side of the equation above is a constant for any given V.

2. For the potential curves, near the Schottky contact, all the curves are close together; near the edge of depletion region they deviate from one another by no more than 2kT/q. Also they are close to the potential curve found from the depletion approximation.
3. For electron concentration, all the curves meet near the edge of depletion region with electron concentration approximately equal to 50 % of N_d . The total charge Q in the depletion region for each curve, is equal to $\varepsilon(\frac{d\psi}{dx})_0$ multiplied by the diode area, which is the same as in the depletion approximation.

Thus, although the detailed shape of the depletion region differs from that predicted by the depletion approximation, so little charge is displaced that only negligible effects on the field (and hence the potential) are observed. This displaced charge, however, will be seen to have more significance when we wish to explain the properties of the Gap diode in the next chapter.

3.5 TWO-DIMENSIONAL SIMULATION

With 64 K-bytes of memory, the maximum number of nodes available for calculations is about 81. Under this limitation one has to suitably define the meshes over the entire area. All the node information is stored on the disk along with subprograms, intermediate data, etc.. Most of the computing time is used in calculating the inverse matrices of equations 3.10 and 3.14.

If the relationship between D_n and μ_n is close to the Einstein relationship or $D_n / \mu_n \simeq$ constant, the following arrangement can be applied to simplify the simulation: The current equation may be rewritten as:

$$J_n/q \simeq D_n \exp\left(\frac{\mu_n}{D_n} \psi\right) \nabla\left[n \exp\left(-\frac{\mu_n}{D_n} \psi\right)\right] \tag{3.28}$$

If

$$\frac{n}{N_d} \exp\left(-\frac{\mu_n}{D_n} \psi\right) \equiv \phi$$

is defined, equations 3.1 and 3.28 become:

$$\nabla^2 \psi = \frac{q}{\epsilon} N_d \left[\phi \exp\left(\frac{\mu_n}{D_n} \psi\right) - 1\right] \tag{3.29}$$

and

$$J_n/q \simeq D_n \exp\left(\frac{\mu_n}{D_n} \psi\right) N_d \nabla\phi \tag{3.30}$$

respectively. Now the variables are ϕ and ψ instead of n and ψ. The simulation procedures are the same as that described previously. The advantage of this is that it is easier to handle the boundary values this way and the calculation is simplified. In most of the cases, it is possible to adjust the value of ϕ to be in the range of 0 to 1, in order to obtain accuracy and convergence. Also, the current has the same direction as $\nabla\phi$, so one can easily predict the current direction at each node. This also helps to check if the simulation results are physical.

In the next two chapters two simulation examples and their results are shown.

4. GAP CONTROLLED METAL-SEMICONDUCTOR DIODE

In this chapter, a new metal-semiconductor device is described whose I-V characteristic is controlled by a geometric gap between adjacent Schottky metal regions.

4.1 CONFIGURATION

Consider the cross-sectional view shown in Figure 4.1. The device represented there consists of an n-type epitaxial layer of GaAs on an N^+ conducting substrate. Stripes of a Schottky metal are deposited either on the surface or in notches in the epi-layer. Thus, a gap exists between adjacent Schottky barrier regions exposing the n-layer. Finally, an ohmic contact is established over the entire surface, connecting the Schottky barrier regions and the n-layer filled gap in parallel. Note that this cell can be repeated across the surface of a wafer. We term this configuration the Gap diode.

4.2 COMPUTER SIMULATIONS AND ANALYSIS

The parameters used in the device simulation are listed as follows:

built-in potential	$\phi_b = 0.72$ V
doping concentration	$N_d = 2\text{x}10^{15}$ cm^{-3}
energy relaxation time	$\tau_e = 10^{-13}$ sec
saturated Velocity	$V_s = 2\text{x}10^{7}$ cm/sec
critical field	$E_o = 3.2$ KV/cm
diode height	$l_2 = 0.81$ μm

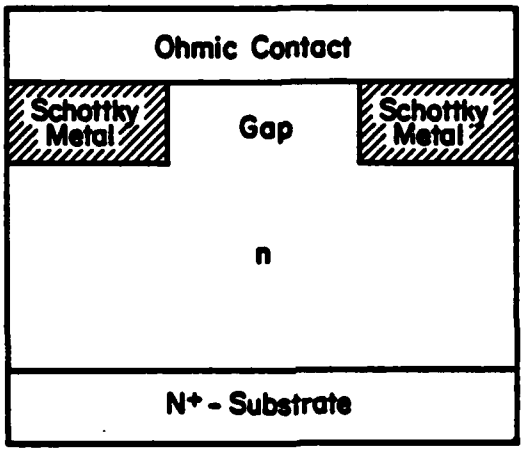

Figure 4.1 Cross-section of the Gap Diode. Typical device parameters: $N_d = 2 \times 10^{15} cm^{-3}$; gap width = 1 μm; epi-layer thickness = 1 μm ; diode area = $8 \times 10^{-6} cm^{-2}$.

gap width	d_1 = 0.72, 1.08, 1.44μm
aspect ratio	d_1/l_1 = 8/11
Schottky height	d_2 = 0.36 μm
diode area	$l_1 l_3$ = 8×10^{-6} cm^2
depletion length	W_o = 0.706 μm

The configuration is shown in Figure 4.2.

The simulation procedures and techniques have been described in Chapter 3. Figure 4.3 shows the mesh lines and the Schottky contacts denoted by filled dots. Note that the entire area can be separated into two symmetrical parts. Therefore, only the upper half is simulated. The open circles represent the ohmic contacts and the crosses, the noncontact boundaries. This information is entered in Program 1 of the appendix. For example: In line 41, "I" denotes nodes inside the semiconductor. In line 40, "B" denotes nodes on the boundaries. Following this, line 61 asks whether the node is on the Schottky contact or the ohmic contact, etc. In the same program, the following information is also given: the mesh spacing (lines 25-28, 57-60), the adjacent nodes (lines 51-54), geometry structure control (lines 35, 90-111), and material parameters including doping concentration, barrier height and electron mobility (all in line 32). Finally all node information is stored in a file named Cnode (lines 71-74), and all others in Cinp (line 112) and CJ# (line 127), here file CJ# is for current density input and output control.

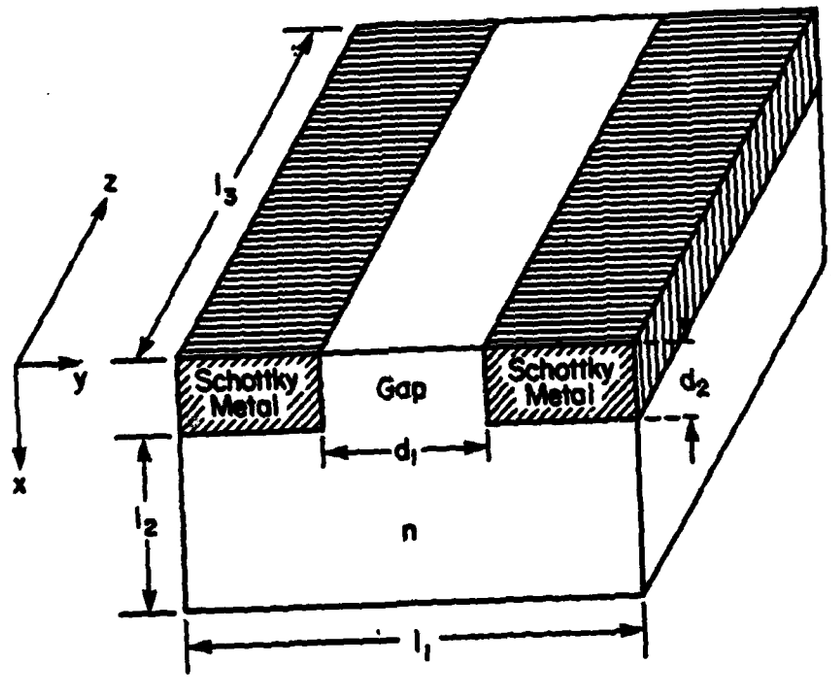

Figure 4.2 The significant region of Gap diode used in simulation. d_1 and d_2 are used as two control variables.

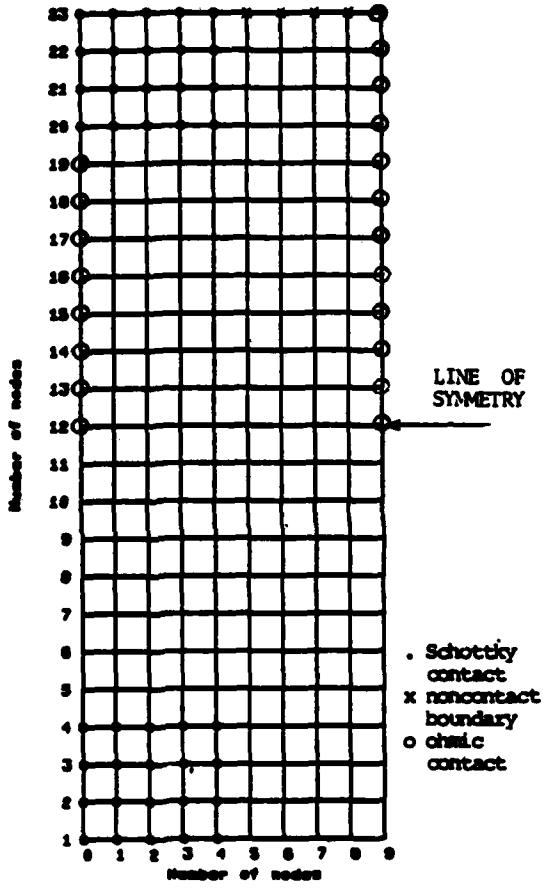

Figure 4.3 Mesh lines used in simulation.
Only the upper half including the symmetry line is involved in the simulation.

Boundary value assignment is set in the main program (lines 17-26, Program 3 in the appendix).

A typical printout of the computer results is shown in Figure 4.4. The first part is the potential value at each node. The second is the coreesponding carrier concentration normalized to doping concentration. The printout has been designed to have the same appearance as Figure 4.3. Also, the current density at each node on both sides is given to help in understanding the current conduction. Finally, the average current density on the bottom line multiplied by the diode area is the total current. The average current density values on the input and output sides also serve as a check of the quality of the simulation. Notice that the round-off error might limit the precision.

From these numerical results, iso-electron concentration and equi-potential plots can be drawn, as shown in Figures 4.5 and 4.6. Note that the curves near the corners of gap area adjacent to the Schottky metal are not precise, because of the uncertainty for the boundary values. These two figures give some insight into how the diode works.

The principal of operation is as follows. At zero bias the Schottky metals deplete the semiconductor both below the contacts themselves and in the gap between them. By adjusting the width of the gap and the depth of the

```
          dVi= 1.290E-02
          dVi= 9.667E-03
          dVi= 1.958E-03
          dVi= 2.773E-04
          dVi= 5.068E-06
 Applied Voltage=      0.630
dx=0.0000E-06cm     dy=0.0000E-06cm
                Generalized Mobility and Velocity
        Relax. time=  1.00E-13sec
       Vi=
                                  -0.600 -0.505 -0.344 -0.207 -0.092  0.000
                                  -0.600 -0.497 -0.338 -0.213 -0.115  0.000
                                  -0.600 -0.470 -0.320 -0.214 -0.170  0.000
 -0.600 -0.600 -0.600 -0.600 -0.600 -0.429 -0.273 -0.170 -0.098  0.000
  0.630 -0.280 -0.380 -0.427 -0.405 -0.297 -0.197 -0.119 -0.057  0.000
  0.630 -0.121 -0.207 -0.240 -0.230 -0.181 -0.124 -0.073 -0.033  0.000
  0.630 -0.042 -0.094 -0.119 -0.118 -0.097 -0.067 -0.038 -0.017  0.000
  0.630 -0.003 -0.031 -0.047 -0.050 -0.042 -0.030 -0.017 -0.008  0.000
  0.630  0.015  0.001 -0.008 -0.013 -0.012 -0.009 -0.005 -0.002  0.000
  0.630  0.022  0.015  0.008  0.004  0.002  0.001  0.001  0.000  0.000
  0.630  0.025  0.020  0.015  0.011  0.008  0.005  0.003  0.002  0.000
  0.630  0.025  0.021  0.016  0.012  0.009  0.006  0.004  0.002  0.000
                                 Last line is Symmetric Axis
       Ni=
                                  0.000  0.000  0.000  0.003  0.000  1.000
                                  0.000  0.000  0.000  0.002  0.030  1.000
                                  0.000  0.000  0.000  0.001  0.013  1.000
 0.000  0.000  0.000  0.000  0.000  0.000  0.001  0.007  0.063  1.000
 1.000  0.002  0.000  0.000  0.000  0.000  0.004  0.027  0.167  1.000
 1.000  0.015  0.002  0.001  0.002  0.005  0.021  0.092  0.332  1.000
 1.000  0.085  0.024  0.014  0.019  0.030  0.088  0.240  0.529  1.000
 1.000  0.309  0.144  0.103  0.115  0.173  0.291  0.473  0.714  1.000
 1.000  0.590  0.407  0.348  0.358  0.429  0.549  0.688  0.864  1.000
 1.000  0.813  0.682  0.637  0.642  0.683  0.771  0.865  0.932  1.000
 1.000  0.916  0.867  0.827  0.827  0.851  0.888  0.930  0.967  1.000
 1.000  0.943  0.904  0.883  0.882  0.898  0.923  0.951  0.977  1.000
                                 Last Line is Symmetric Axis

Current dens. in                                  Current dens. out
  2.497E-04                                         2.774E-02
  3.383E-04                                         5.121E-02
  6.388E-04                                         2.901E-01
  2.714E-03                                         2.048E 00
  9.738E-03                                         1.103E 01
  4.852E-01                                         5.288E 01
  1.749E 01                                         1.649E 02
  1.288E 02                                         2.981E 02
  3.884E 02                                         4.291E 02
  6.394E 02                                         5.381E 02
  7.888E 02                                         6.887E 02
  8.219E 02                                         8.219E 02
                    Average Current Dens.
  2.898E 02                                         2.898E 02
```

Figure 4.4 Typical printout of computer results.

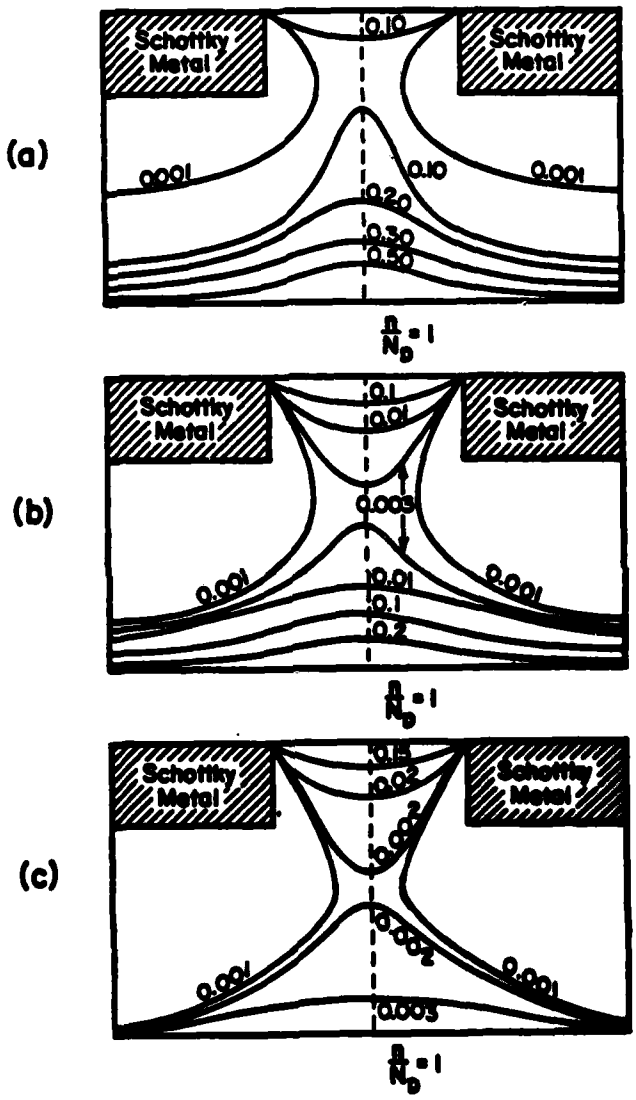

Figure 4.5 Normalized electron concentration contours for one-depletion-length Gap diode.
(a) forward bias : 0.3 V (b) zero bias
(c) reverse bias : -0.3 V.

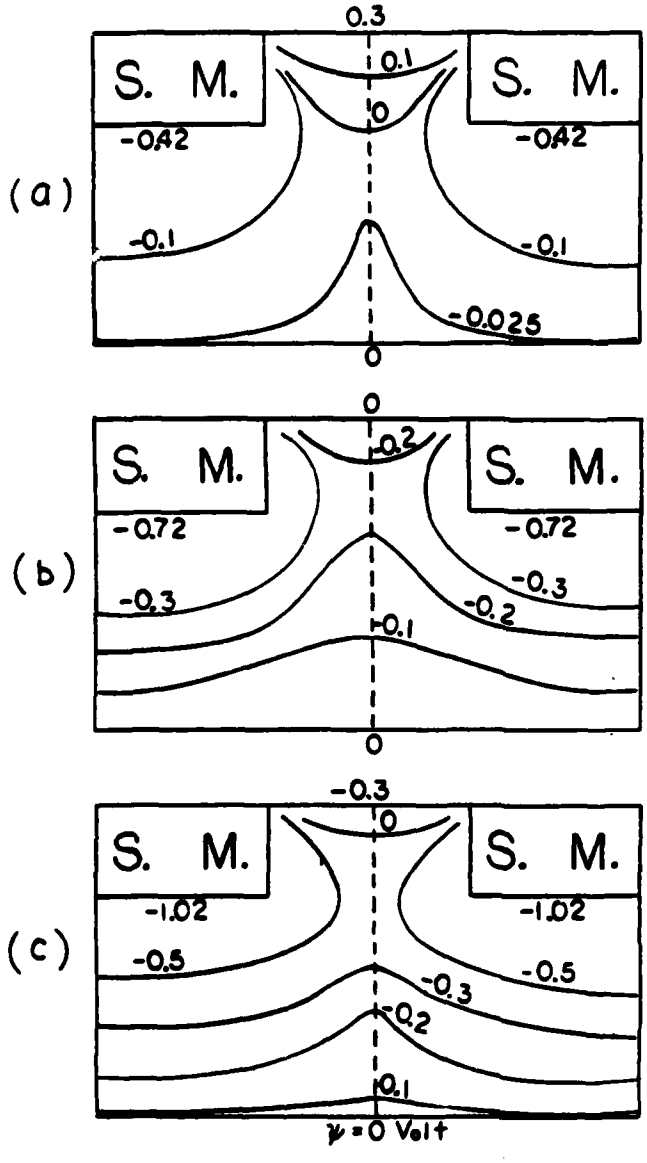

Figure 4.6 The corresponding potential contours of Figure 4.5.

notch, the turn-on voltage for a given doping and choice of metal can be set. For example, Figure 4.5 (b) shows contours of equal free charge concentration, n, normalized to the doping concentration, N_d, with no bias applied. Note the heavily depleted regions under the Schottky contacts and up into the gap as well. In reverse bias, Figure 4.5 (c), the depletion regions punch through to the cathode contact and the neck between the depletion regions moves down from the gap. Reverse leakage current is supported by the large number of free carriers in the gap and in the neck between the depleted regions. In forward bias, Figure 4.5 (a), the depletion regions are retracted toward the metal contacts, thus exposing an ohmic channel for charge carrier conduction. Notice that this occurs for forward bias well below that needed to draw current through the Schottky contacts. This can be seen in the current density results in Figure 4.4, which also shows the effect of current spreading at the cathode contact.

It can be understood through the one-dimensional simulation in Chapter 3 that the edge of the depletion region is not so sharp as predicted by the depletion approximation. The displaced charge between the two depletion regions in the gap explains why forward conduction through the gap is much easier than through the Schottky contact. This also explains why the reverse current is much higher than in a conventional Schottky

contact. However, the reverse current, in general, is much less than the forward current, since the depletion region spreads into the gap in reverse bias.

Current - Voltage characteristics for the Gap diode are shown in Figure 4.7. Here the parameter is the gap width normalized to the zero bias depletion length, Wo. The right-most curve is the result for a conventional SBD. Note that, as expected, the turn-on voltage can be set from nearly the built-in potential down to nearly zero. However, as the gap is widened the reverse current is increased.

Figure 4.8 shows the corresponding I-V curves in log scale. For comparison, a pure resistor which is equivalent to a gap diode with a very wide gap length, say four depletion lengths or more, is presented. Note that the Schottky diode I-V curve is a straight line in log scale. As the gap length increases, the curvature changes correspondingly. When the gap width exceeds two depletion lengths the I-V curve will converge to that of a resistor. Thus, the shape of the Gap diode I-V curve is also controllable by adjusting the gap length. For different applications, different requirements on the turn-on voltage and I-V curvature might be preferred. Then the optimization of the gap length, designed to satisfy a special application, will deserve to be studied in further detail.

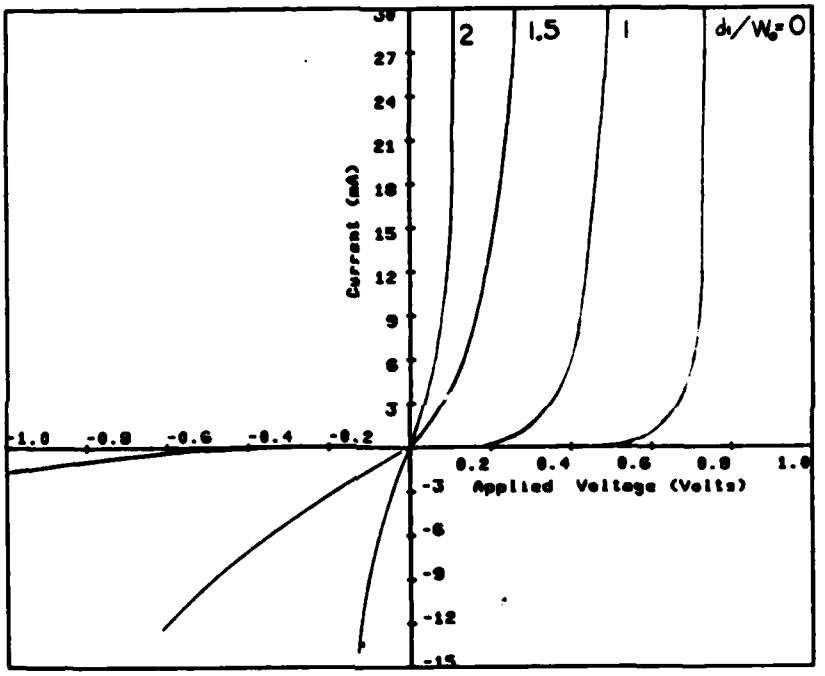

Figure 4.7 Predicted I-V characteristics with the normalized gap width as the parameter.

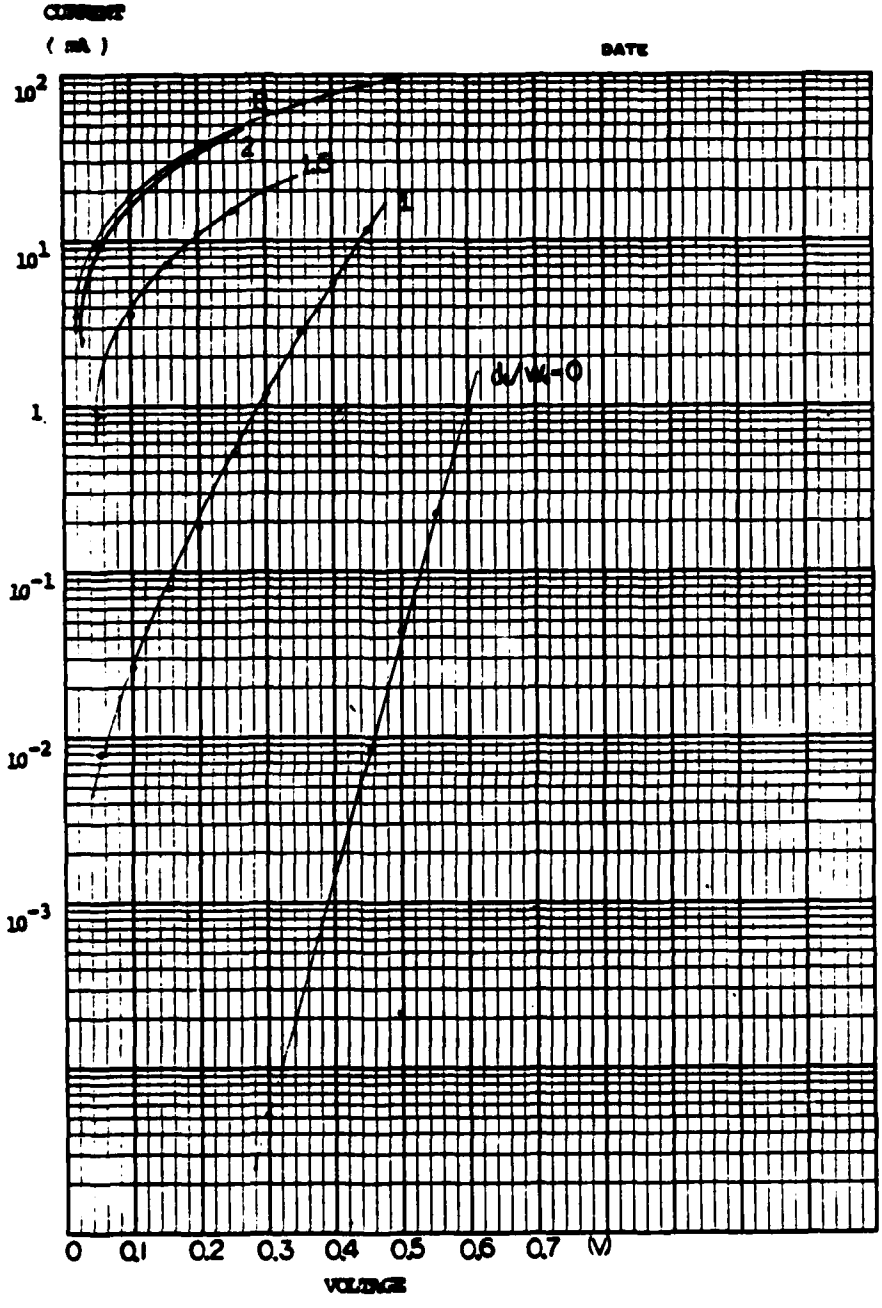

Figure 4.8 The corresponding I-V curves of Figure 4.7 in log scale. For comparison a corresponding resistor (R) is also shown.

Figure 4.9 shows predicted I-V curves using the depth of the notch d_2 as the control variable. Thinner notches correspond to lower turn-on voltages. Note that even for $d = 0$, the I-V curve is still controllable by adjusting the gap length. This is the planar-type Gap diode.

The capacitance can be calculated from

$$C = \left|\frac{dQ}{dV}\right| = \frac{1}{\Delta V}\left|\frac{1}{\ell}\sum_{\ell=1}^{\ell}(N_d-N_i)_V^{V+\Delta V}\cdot l_1 l_2 l_3\right| \qquad (4.1)$$

Here, ℓ and N_i are defined in Chapter 3. $l_1 l_2 l_3$ is the volume of the bulk semiconductor region. The predicted capacitance - voltage relation is shown in Figure 4.10. Before turn-on, the capacitance of the Gap diode is lower than that of the same size Schottky diode. This is because most of the current goes through the gap instead of the Schottky metal contact. When the bias voltage approaches the turn-on voltage, which is approximately 0.46 volts in this case, the capacitance increases rapidly. For the Gap diode, the current conduction can be considered as being controlled by an equivalent potential barrier in the gap. Its value is close to the turn-on voltage. Recall that the capacitance is defined in equation 2.12. When the applied bias approaches the turn-on voltage, W becomes very small and the capacitance increases very quickly. Note that in Figure 4.10 the SBD

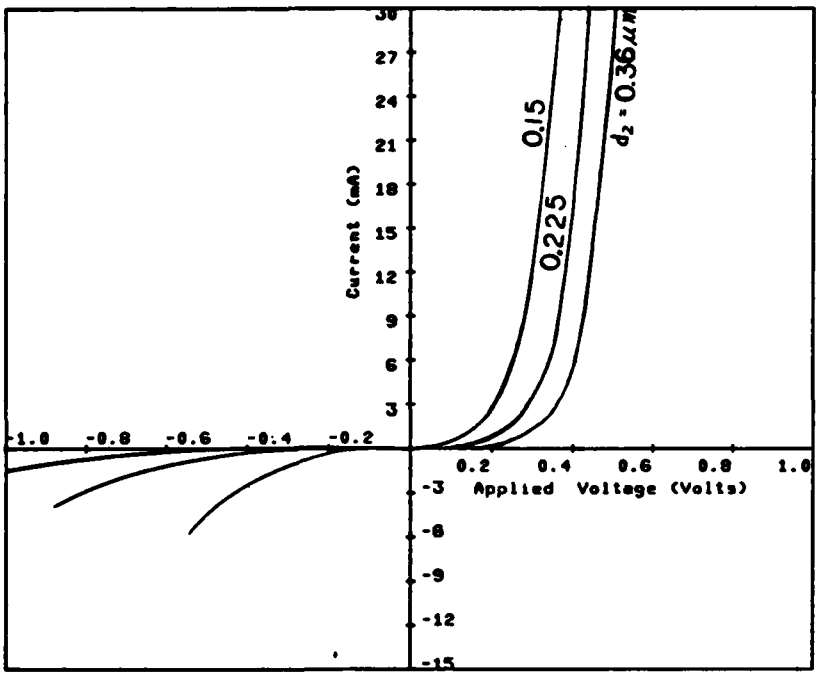

Figure 4.9 Predicted I-V curves using (notch thickness), d_2, as the parameter. All other parameters stay the same as before.

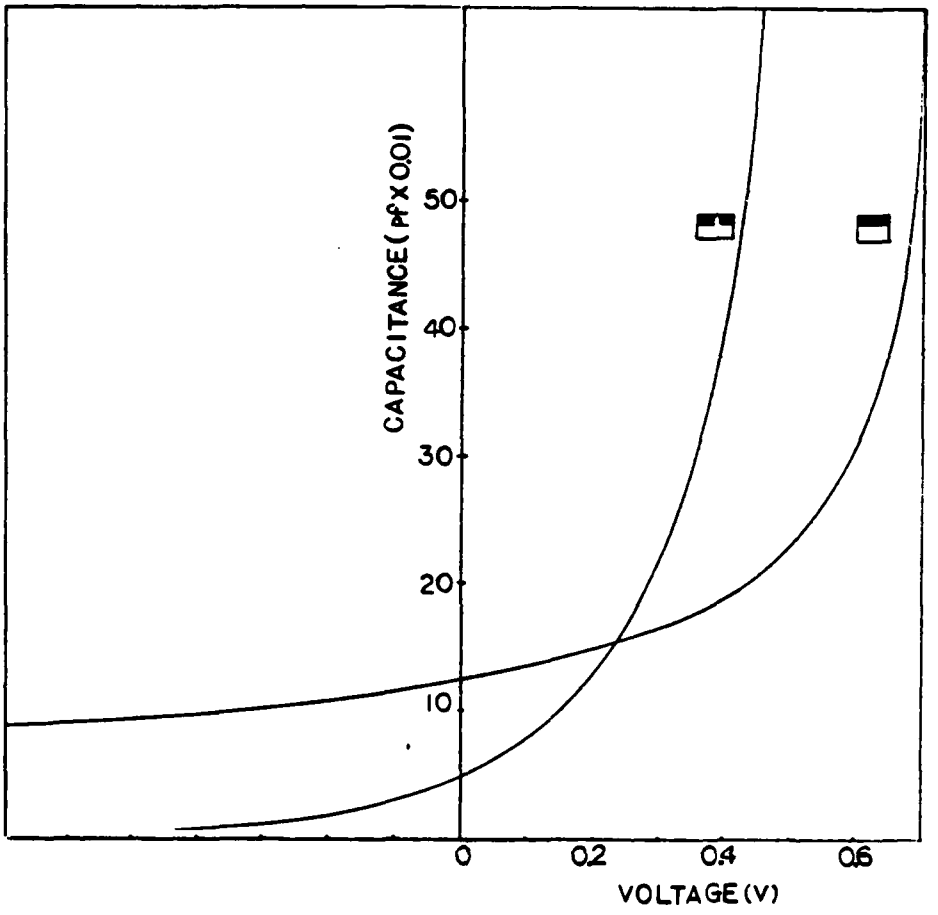

Figure 4.10 C-V curve of a Gap diode with a one depletion length gap in comparison with a corresponding Schottky-barrier diode.

was assumed to have infinite length. However, the length of the Gap diode is approximately one-depletion length. Therefore, in the reverse bias case, the C-V curve of the Gap diode approaches a low value rapidly due to punch-through and the conduction modulation effect of the gap.

4.3 EXPERIMENT

Experiments with this new device have been reported by Teng et al. (37). Figure 4.11 shows the experimental I-V characteristics for diodes with seven different gap widths. The right hand curve is for a Schottky diode with a 30 μm diameter, the same as that of the Gap diodes. Note the striking similarity to the predicted I-V curves of Figure 4.7.

4.4 COMMENTS

1. Effort has been expended to find an analytical expression for the I-V relation. One way to treat this problem is to apply the potential barrier concept on the gap region and consider the entire diode as a parallel combination of the Schottky-barrier region, rectifing gap region and perhaps the ohmic gap region if the gap is comparatively large. There is no difficulty in finding the I-V relation for the Schottky barrier region. However, because of the narrow gap nature, it is difficult to obtain an suitable expression for the current through the gap.

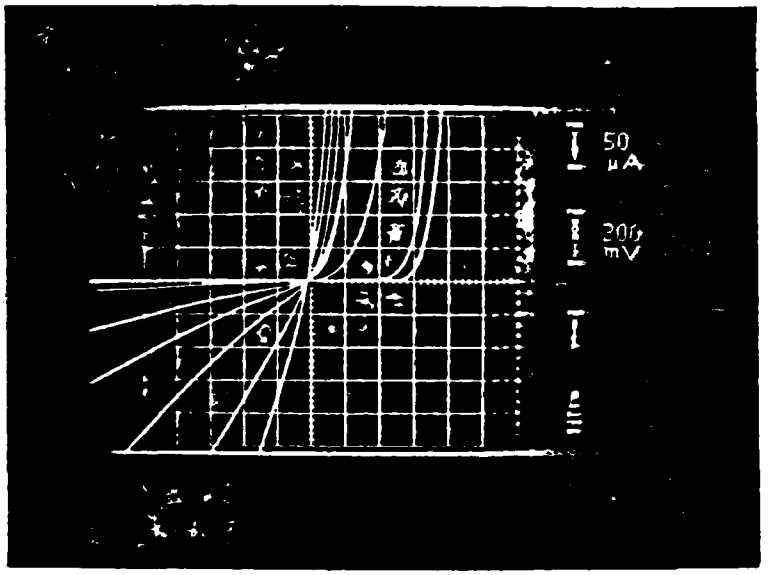

Figure 4.11 Experimental I-V characteristics for diodes with seven different gap widths. Right hand I-V curve is for pure Schottky-barrier diode.

2. In the gap, since both Schottky contacts have the same potential, therefore, right underneath the ohmic contact there should be some depletion area on both sides. Because of the properties of Poisson's equation, the transitional depletion edge may stretch out to as much as two Debye lengths. Also, because of the interaction between the two adjacent depletion regions, the total controllable gap length might be as much as

$$W_o + 2L_{Debye} + \delta + 2L_{Debye} + W_o \simeq 3\ W_o \qquad (4.2)$$

where δ is of the order of one Debye length. Note that

$$W_o/L_{Debye} = \left[\frac{V_o}{kT/Q}\right]^{1/2} \simeq 5.27 \qquad (4.3)$$

if Vo = 0.72 V.
This is close to what is observed experimentally.

3. We have demonstrated a new device principle: It is possible to produce depletion of carriers under an ohmic contact region. By this means, a large range of turn-on voltages, from that of the pure Schottky to nearly zero volts, can be obtained. This observation can be applied to other two- or three- terminal structures which may yield microwave and mm-wave devices with new and desirable properties.

5. GEOMETRICALLY CONTROLLED ANTISYMMETRIC METAL-SEMICONDUCTOR DIODE

In this chapter the design of an antisymmetric diode is reported. The computer results show that the shape of its I-V curve can be adjusted as well as its turn-on voltage. This new device has possible high frequency applications.

In 1974 Schneider and Snell (48) and Cohn, Degenford and Newman (38) reported simultaneously a new mixer, named the antiparallel mixer diode pair. In this device, because of its antisymmetric configuration (See Figure 5.1 (b)), the I-V curve is symmetrical with respect to the origin. If a local oscillator sinusoidal voltage is applied to this device, there will be two switching cycles for each cycle of the local oscillator voltage. This is double that of the single diode mixer case. It has been shown (38) that the total current of the antiparallel diode pair contains only frequencies $mf_s + nf_o$ for which $m + n$ is an odd integer; f_o and f_s are the frequencies of the local oscillator and the signal, respectively. On the other hand, the single diode mixer results in a diode current having all frequency components. This characteristic property suggests that such a configuration has the advantage as a subharmonic mixer, because it can

be pumped at half of the frequency required for the local oscillator in a single diode mixer.

The natural suppression of the fundamental and other mixing products is lessened due to the slightly nonidentical electrical properties of the two diodes for the antiparallel diode mixer pair, such as differences in saturation currents and I-V curvatures (38). Furthermore, although the diodes may be identical, since they are physically separated their circuit environments may not be identical. Therefore, the overall electrical characteristics of the antiparallel mixer diode pair may not be symmetric. This also results in the incomplete suppression of undesired mixing terms. So the conclusion is that one needs good electrical symmetry as well as mechanical symmetry for proper device operation (49). Due to practical considerations, this is especially hard to accomplish at mm-wavelengths (50).

Also mentioned by Cohn et al. (38), the suppressed current components circulate within the loop formed by the two diodes. According to Kerr (49), the magnitude of the loop inductance, as seen by currents circulating through the two diodes, strongly affects the subharmonically pumped mixer performance, such as conversion loss and noise figure in mm-wave applications. Therefore, adjusting this loop inductance to optimize the performance is an important topic to be considered.

In 1978, Cardiasmenos reported a successful technique to fabricate such a device with a 5-dB DSB noise figure at 94 GHz (50). These planar type devices are used in suspended stripline substrates. Microprocessor-controlled machinery replaces the traditional trial and error fabricating and trimming work and achieves highly reproducible results. The entire fabrication procedure is very complicated and this is believed to be the first successful report on the mass production of the antiparallel mixer diode pair.

In order to explore alternative means of realizing the desired I-V characteristics, we consider an innovative design for such device in the following:

5.1 CONFIGURATION AND PHYSICAL ANALYSIS

Consider the geometry of Figure 5.1 (a). A Schottky metal, such as A. is deposited over a portion of an N+ substrate, and N-doped GaAs layer is grown around and over it. After the desired diode thickness is obtained a second Schottky metal is deposited over the antisymmetric side and finally an ohmic contact is applied to the entire upper surface, completing the device. We call this device the antisymmetric diode. The equivalent circuit of the device is shown in Figure 5.1 (b) which is the antiparallel diode pair. The technology needed to fabricate such a device is the same as that used in the permeable base transistor (51).

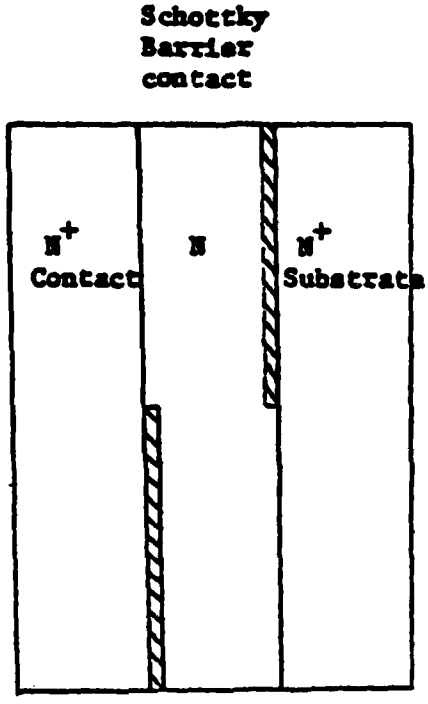

(a) Antisymmetric diode configuration.

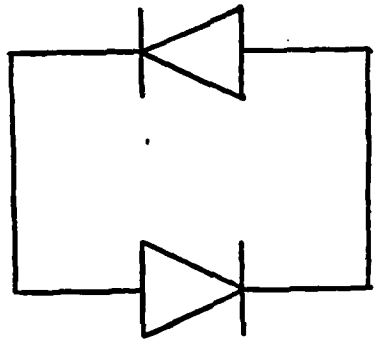

(b) Equivalent circuit - antiparallel (back-to-back) diode pair.

Figure 5.1 Antisymmetric diode and its equivalent circuit.

Such a structure should be highly symmetric and uniform so that well balanced I-V curves should be obtained. Furthermore, the millimeter wave parasitic circuit elements are all external to the new diode so that circuit balance should be improved and impedance matching simplified. In addition to the mechanical and electrical advantages of this structure it can be shown that, with the barrier height unchanged, the turn-on voltage can be lowered to a suitable value.

5.2 COMPUTER SIMULATIONS AND ANALYSIS

Using the techniques described in Chapter 3, the computer simulation for this configuration has been carried out for a device with the parameters given below:

doping concentration	$N_d = 1 \times 10^{17}$ cm^{-3}
built-in potential	$V_o = 0.72$ V
diode height	$l_x = 0.1064$ μm
overlap length	$l_o = 0.0266, 0.02, 0.0133$ μm
diode area	$l_y l_z = 1 \times 10^{-5}$ cm
electron mobility	$\mu_n = 5000$ cm^2 V^{-1}sec^{-1}
overlap ratio	$l_o/l_y = 1/5$
depletion length	$W_o = 0.0998$ μm

The configuration used in simulation is shown in Figure 5.2. Here, N_d is the doping concentration for the bulk semiconductor, and l_x is the thickness of the bulk region. The two Schottky metals overlap by l_o. In order to simplify the simulation, the Einstein relationship is

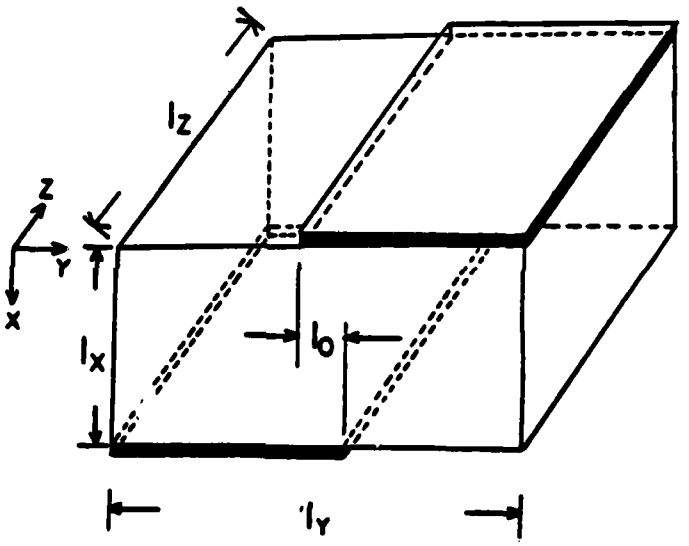

Figure 5.2 The active region of the antisymmetric diode used in the simulation. *Only the x-y cross-section is considered.*

assumed. Because of the antisymmetric geometry, it is necessary to analyze only one polarity of applied bias voltage. In the z-direction the diode structure is assumed uniform, therefore only a two-dimensional simulation is performed.

Figures 5.3 and 5.4 show the carrier concentration and potential contours, respectively, for a typical antisymmetric diode. With zero bias, i.e. graph (b) of Figures 5.3 and 5.4, the geometric symmetry of the diode is reflected in the contours. The electron concentration is normalized to the doping concentration N_d. Areas where the contour values are less than $n/N_d = 0.001$ are considered to be depleted. The area next to each Schottky metal contact is depleted. This phenomenon is similar to that observed in the one-dimensional case. Assuming that the length of the depletion region surrounding each metal contact is approximately equal to one depletion length, if the thickness of the bulk region, i.e. the distance between the two Schottky metal contacts, is of the order of two depletion lengths, then it is expected that there is no undepleted channel between the two ohmic contacts under zero bias (See Figure 5.3 (b)). When a small bias is applied (Figure 5.3 (a)), since the left hand Schottky contact is forward biased, the corresponding depletion region is retracted toward the metal. At the same time, the other Schottky contact is reverse biased, and so the

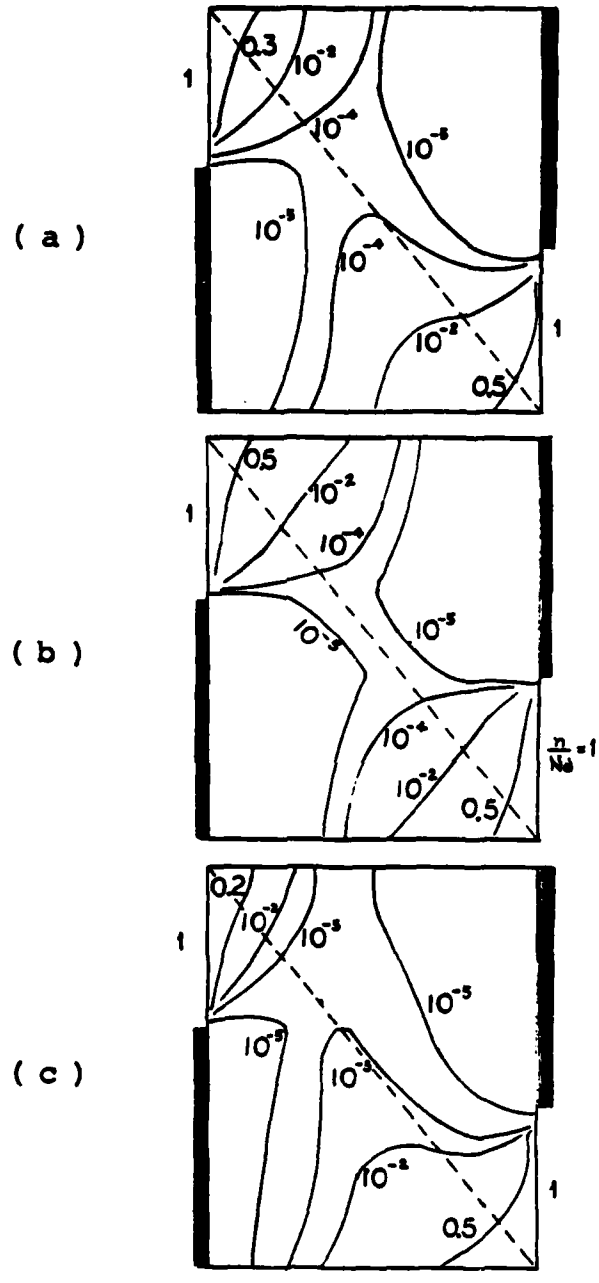

Figure 5.3 Typical electron concentration contours for the antisymmetric diode. (a) V = 0.15 volt, n increases in the central region (b) V = 0, the contours are symmetrical (c) V = 0.30 volt, electron conduction through the central region turns the diode on.

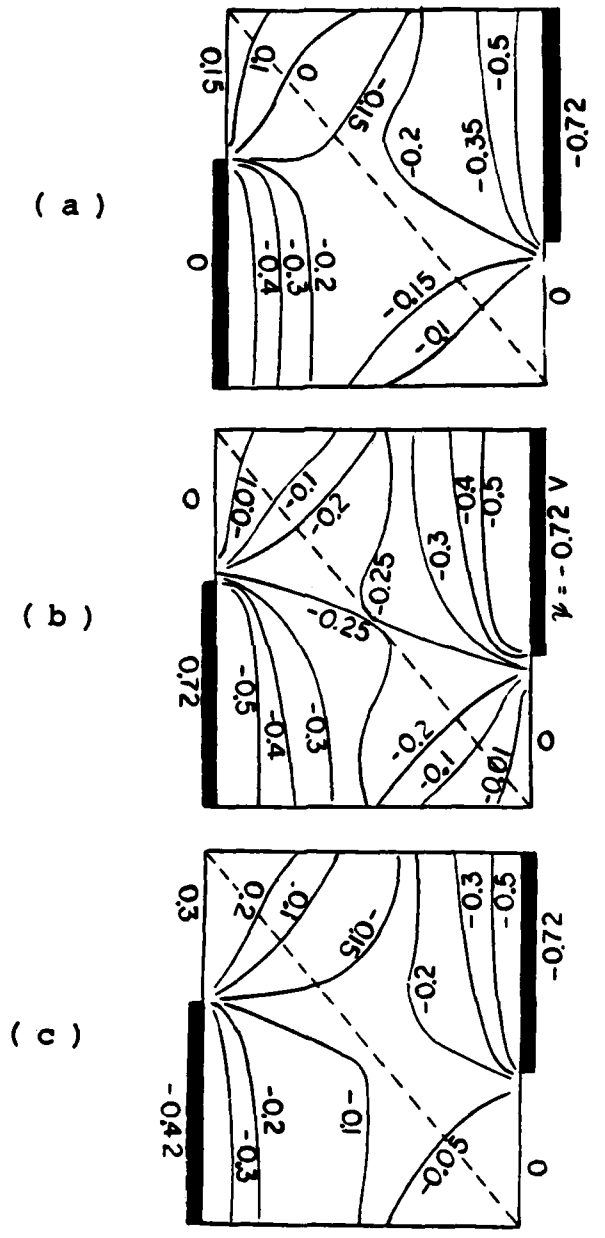

Figure 5.4 The corresponding potential contours of Figure 5.3.

corresponding depletion region extends further out into the bulk material. Comparing this with the zero bias case, it is observed that in the central region, the electron concentrations increase. This phenomenon is more clearly observed in Figure 5.3 (c) which shows an exposed ohmic channel for electron conduction. In fact, the diode is already turned on. Notice that this occurs for a bias voltage well below that needed to turn on the SBD. Instead of carrier conduction through the metal contact, this new conductivity modulation device provides a voltage variable ohmic channel for conduction. It will be shown later that the I-V relation is exponential for both polarities of applied bias.

Figure 5.4 shows the corresponding potential contours for reference. Similar to the Gap diode, because of the uncertainty of boundary values, it is difficult to accurately describe areas where the Schottky metal contacts meet the ohmic ones. Away from these areas, along the metal contacts, the potential becomes more and more uniform. From these contours, the electric field can be found. In order to obtain an accurate picture of the current density distribution not only the electron contour plot but also the potential contour plot must be taken into account (See equation 3.2).

Figure 5.5 shows I-V curves for different [illegible] the Schottky metal. Also shown, for compar[illegible]

AD-A120 484 NUMERICAL ANALYSIS OF SEMICONDUCTOR DEVICES USING MICROCOMPUTERS(U) WASHINGTON UNIV ST LOUIS MO DEPT OF ELECTRICAL ENGINEERING P S CHEN ET AL. JUL 82 2/2

UNCLASSIFIED TR-82-3-ONR N00014-79-C-0840 F/G 9/1 NL

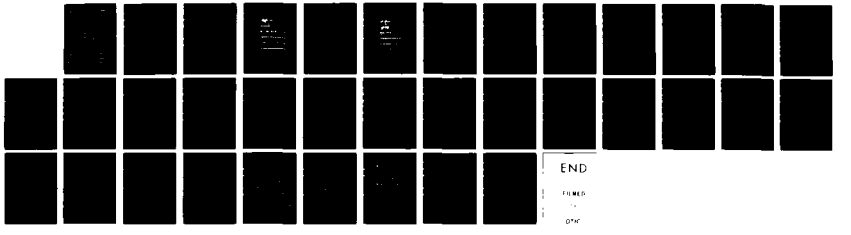

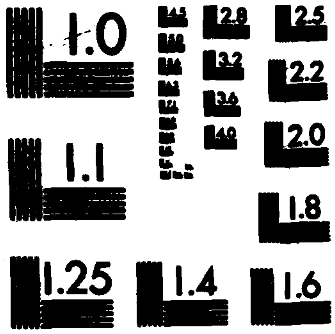

MICROCOPY RESOLUTION TEST CHART
NATIONAL BUREAU OF STANDARDS-1963-A

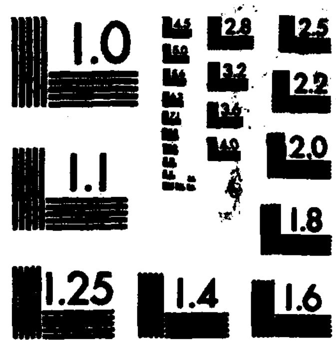

MICROCOPY RESOLUTION TEST CHART
NATIONAL BUREAU OF STANDARDS-1963-A

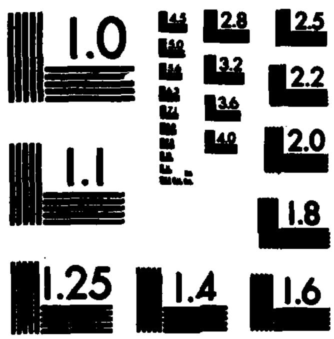

MICROCOPY RESOLUTION TEST CHART
NATIONAL BUREAU OF STANDARDS-1963-A

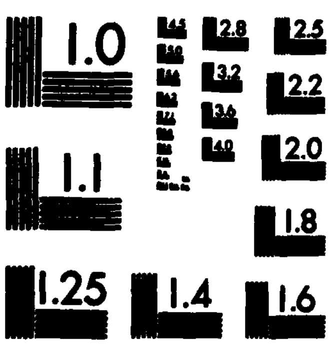

MICROCOPY RESOLUTION TEST CHART
NATIONAL BUREAU OF STANDARDS-1963-A

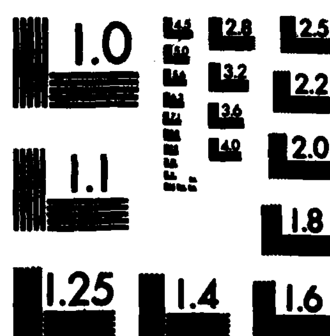

MICROCOPY RESOLUTION TEST CHART
NATIONAL BUREAU OF STANDARDS-1963-A

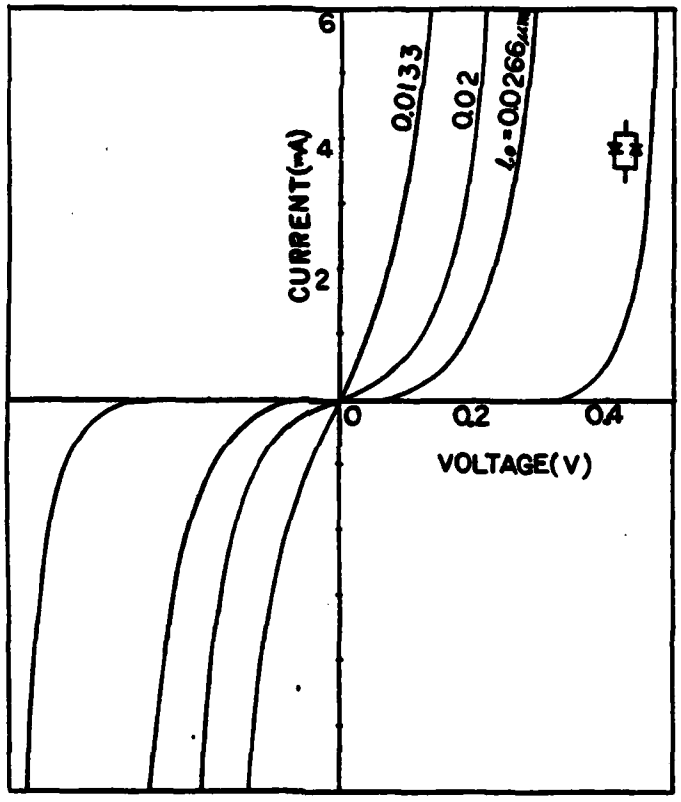

Figure 5.5 Computer results of I-V curves with the overlap, l_o, as control parameter. For comparison, a corresponding back-to-back diode pair I-V curve is also shown.

I-V curve for a conventional back-to-back SBD pair with V. = 0.72 V. This graph shows that the turn-on voltage responds sensitively to the change of the overlap. More overlap results in a higher turn-on voltage. Figure 5.6 shows the corresponding curves on a log scale. Straight lines in this graph indicate that the I-V curve of the device is exponential, independent of overlap. Moreover, the slopes differ from the back-to-back SBD pair. With the thickness of epi-layer as a parameter, the resulting I-V curves are shown in Figure 5.7. For a thin device, the channel is tightened up and electron conduction is restricted, resulting in higher turn-on voltage. The corresponding I-V curves in log scale are shown in Figure 5.8. Again, all are exponential but with different slopes.

Figure 5.9 compares calculated capacitances for a typical antisymmetric diode and a corresponding antiparallel diode pair. The capacitance of the antisymmetric diode is much lower, since the current conduction is due to conductivity modulation rather than to the Schottky rectifying effect.

5.3 CONCLUSIONS AND COMMENTS

According to the simulation it can be concluded that, for the antisymmetric diode,

1. The I-V curve is antisymmetric and exponential.
2. The turn-on voltage is adjustable by two parameters:

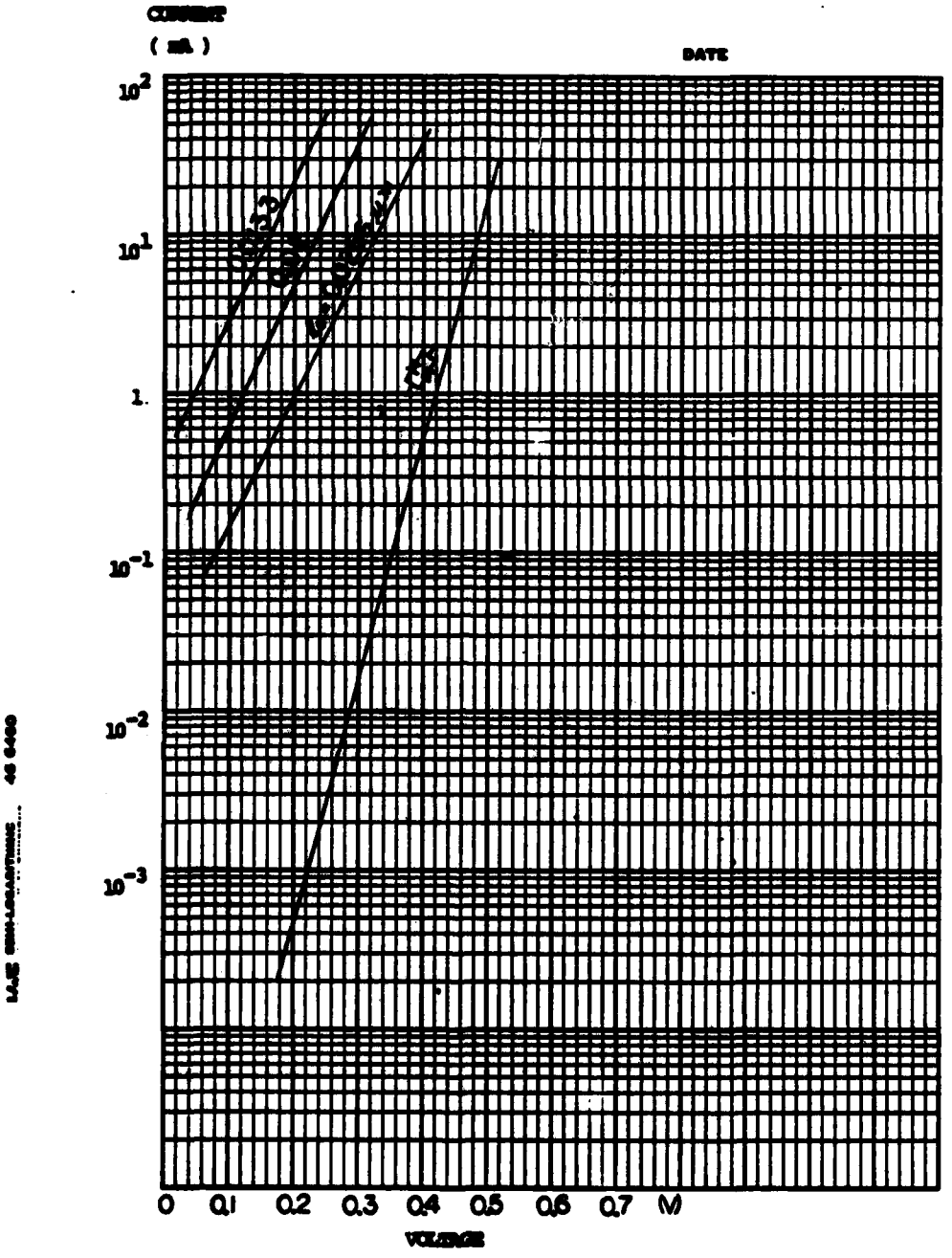

Figure 5.6 The corresponding I-V curves of Figure 5.5 in log scale.

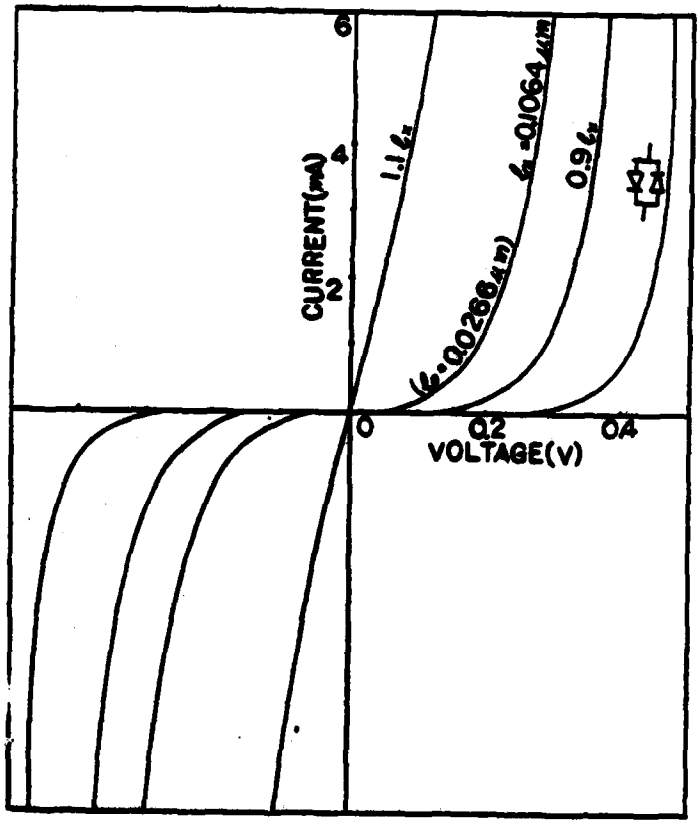

Figure 5.7 Computer results of I-V curves with the epi-layer thickness, l_x, as the control parameter. All other parameters stay the same as before.

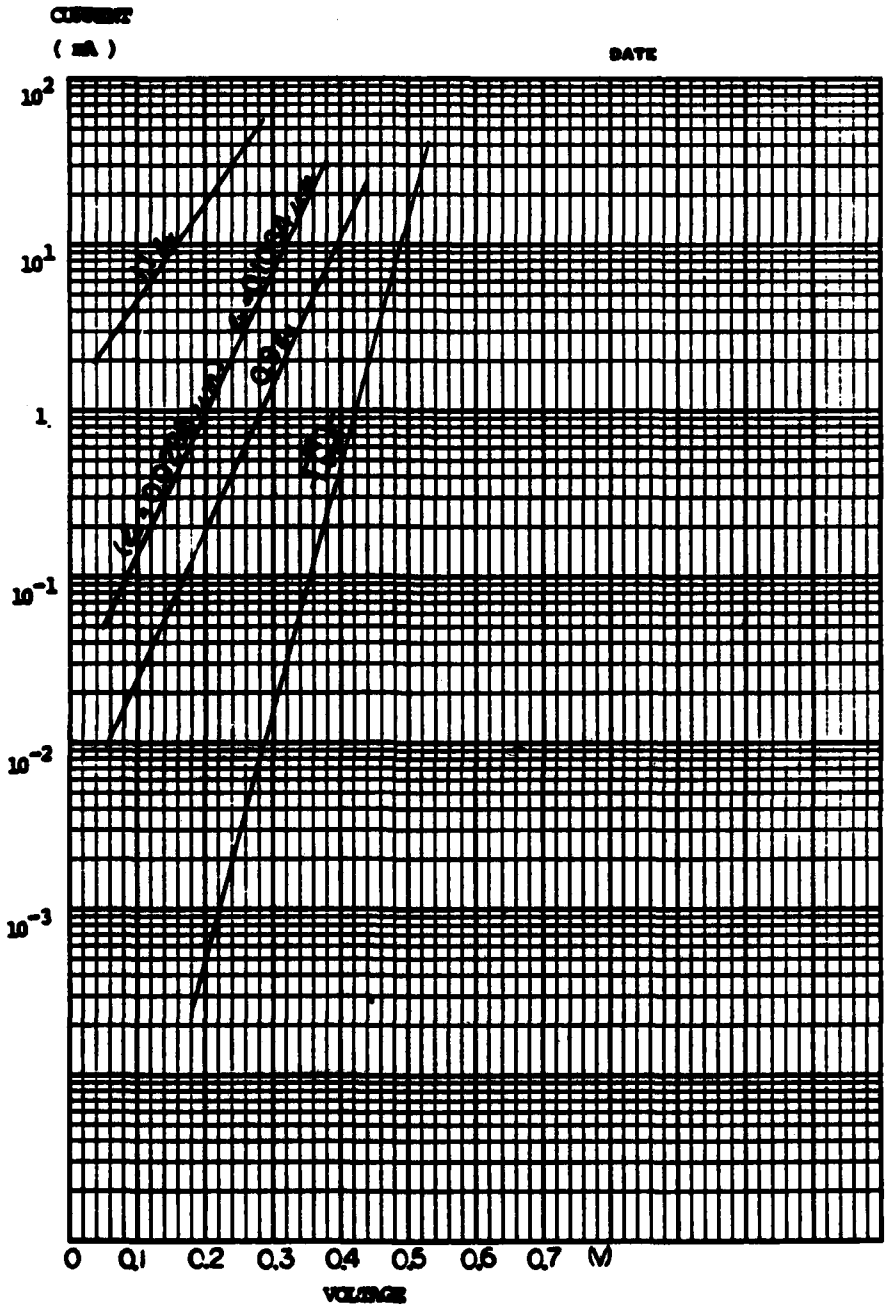

Figure 5.8 The corresponding I-V curves of Figure 5.7 in log scale.

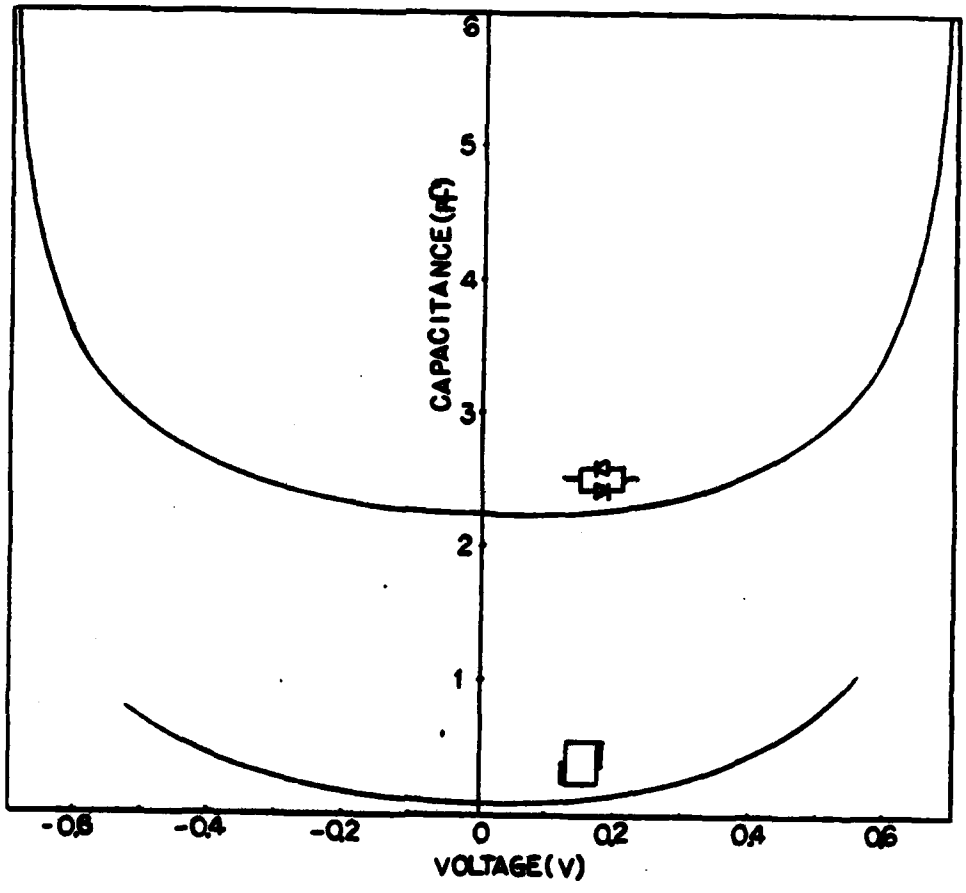

Figure 5.9 Comparison of the capacitance for an antisymmetric diode to a corresponding back-to-back diode pair.

(a) the overlap of Schottky metals.

(b) the thickness of the bulk region.

3. Low capacitance can be expected. Other properties, such as temperature sensitivity and burn-out behavior, should be similar to those experienced with the Gap diode.

From above, the new diode should be useful as a subharmonic mixer and/or limiter.

From the standpoint of design, the thickness of the bulk semiconductor should be no more than 3 depletion lengths. The reasoning is similar to the gap length restriction for Gap diode. Furthermore, the overlap of Schottky metals should not be taken to be too large, since this will produce a low shunt resistance, and the resulting device will be a resistor. On the other hand, too narrow a channel will increase the turn-on voltage and/or capacitance, and the advantage of this new device will be lost.

6. CONCLUSIONS

The purpose of this work is to develop a two-dimensional simulation program capable of modeling the static electrical characteristics of semiconductor devices with complex geometries and made of arbitrary material. The simulation is intended for operation on small (desktop) computers. Another purpose is to use the simulation in the investigation of some new microwave device designs.

6.1 COMPUTER SIMULATIONS

The program that has been developed has the following properties:

6.1.1 User-Oriented program

Information is entered for each node of a mesh which describes the device to be analyzed by the finite difference method. The information to be entered includes the neighborhood node identification numbers, the distances between nodes, and the status of the node (i.e. is it on a boundary, in the interior of the bulk, or on a symmetry line, is it Schottky contact or ohmic contact, is it forward or reverse bias, etc.). The carrier concentration, the potential, and the current density at each node interior to the device can be found as well as the total current for each applied bias voltage.

6.1.2 Modified Decoupled Method

Because of the limited memory available in a small computer, efficient use of this memory is a primary concern. A modified decoupled solution method has been developed using a two stage-iteration scheme which not only saves three quarters of the memory but also yields a converged solution of similar quality to that obtained from the traditional coupled method.

6.1.3 Limitations

The maximum number of nodes available for simulation is limited by the computer memory size. Also, the allowed maximum mesh spacing is dominated by the Debye length. Most of the time consumed in obtaining a solution is used in solving the inverse matrix. Using a small computer, it might take many hours to obtain one I-V curve. However, the trade-off is the low cost of simulation. Since, for a given barrier height, the ratio between depletion length and Debye length is a constant, from the argument above, the total area which can be simulated is limited by the computer memory size. However, usually the area needed for two-dimensional modeling is limited; other parts of the device can be treated by a one-dimensional approximation. Hence it can be concluded that by suitable manipulation, it is possible for the designer to simulate a variety of semiconductor device structures with this program.

6.1.4 Finite Difference And Finite Element Methods

The finite difference method is simple and reliable in programming, and much more effort can be applied to the device simulation itself instead of to debugging the program. Higher order finite element methods might be used to improve the results after a basic understanding of the device under consideration has been made using the finite difference method.

6.2 APPLICATIONS IN TWO-DIMENSIONAL DEVICES

By changing the geometry of the metal-semiconductor diode, we have shown that it is possible to construct a family of new devices which can be used in microwave and mm-wave applications. Based on the simulations, some of the characteristics of two new devices have been predicted.

6.3 GAP CONTROLLED METAL-SEMICONDUCTOR DIODE

In this new design, a simple and effective means by which to control the turn-on voltage of a semiconductor diode has been found. This new contact technique permits the use of conventional Schottky metals and any semiconductor material. This design may also improve the temperature behavior and burn-out rating of these diodes. Furthermore, in fabrication, this diode only takes a few more steps than the conventional SBD, so that the added cost may not be significant. An actual device has been demonstrated in GaAs '37).

6.4 ANTISYMMETRIC METAL-SEMICONDUCTOR DIODE

Another new structure, the antisymmetric diode, was proposed for microwave and/or mm-wave applications. The potential advantages of this device include adjustable turn-on voltage, balance in both polarities, improved burn-out rating, low capacitance and low temperature sensitivity as a mixer or limiter.

6.5 PROBLEMS TO BE SOLVED

Two new types of microwave and mm-wave diodes have been modeled with the technique described in the study presented here. Other configurations also can be investigated. For example, a three terminal device is possible in which the gap technique is used to obtain a vertical FET. A sketch of one such design is shown in Figure 6.1. This is a planar-type vertical FET. Comparing this configuration with that of the Gap diode, as shown in Figure 4.1, the only difference is that on the top portion of this device the Schottky metals are separately contacted to become the gates (G). The drain (D) is formed by an ohmic contact. Apparently, the gate-to-gate length and the epi-layer thickness depend on $V_{..}$ and can be calculated if the gap technique is applied. Because the drain-source distance is much less than for a conventional FET, good performance in high speed and/or high frequency applications can be expected (37,51).

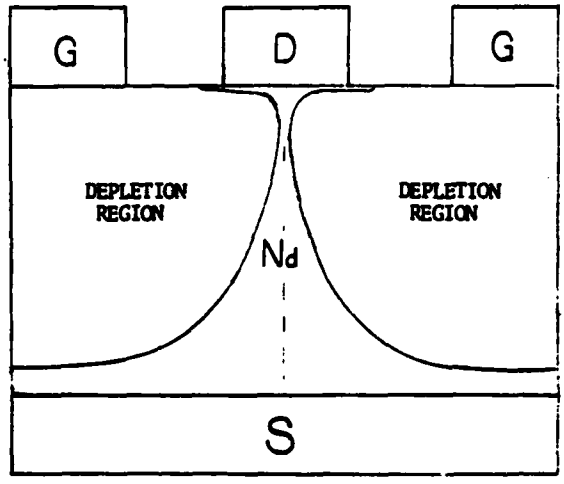

Figure 6.1 Cross-section of planar-type vertical FET. The gate (G), drain (D) and source (S) are of Schottky contact, ohmic contact and N^+ substrate materials respectively. Gates are reverse biased with respect to the drain ($V_{GD} < 0$). The gate-to-gate length and epi-layer thickness depend on V_{GD}. The gap technique can be applied to decide the device parameters (refer to Figure 4.1)

In order to improve the simulation work, other parameters such as temperature should be considered. Refinements of the V(E) and D(E) relations used also would be helpful in obtaining more reliable results. Furthermore, the properties of the contacts should be emphasized since this is an important factor for achieving accurate predictions of device behavior.

With the simple and low cost technique presented here, the simulation of semiconductor device static characteristics is accessible to laboratories with even modest computing capability. Simulations are a powerful tool to aid in the understanding of complex device phenomena. The knowledge so obtained can lead to improvements in existing devices and the exploration of new device concepts.

Finally in this study, it is assumed that the third dimension of the device under investigation is uniform. However, for some small device in which the third dimension is of the order of the other two dimensions, or for which more accurate results are required, it may become necessary to develop three dimensional analysis with a microcomputer.

7. ACKNOWLEDGEMENT

The authors wish to thank Dr. Donald Green for helpful discussions on device modeling; Dr. Kuoh Mee Ling for valuable suggestions regarding numerical techniques; and Douglas Wang for useful information relating to the finite element method. Mr. S.J.J. Teng fabricated the Gap diodes and shared his experimental data. Professor Barbara Shrauner freely provided significant insight into analytical approaches to the one-dimensional case. Finally, we wish to thank Stacie Kawano for her careful reading and editorial help in completing this report.

8. APPENDIX

Program 1 : Node Information

```
0: "General Program for Metal-Semiconductor Diode 6/1/81":
1: drive 0,707;files Cnode,Cinp,CJ0,Cnode-,node00
2: "chan1=c1:input":
3: "chan2=c2:calculation,Since chains to many subprograms,take care of":
4: "the lines when debugging.Something on c-A0":
5: "c-AC=cAC,c-A0=cA0,c-ACm=cACm,c-prt=cprt:subprograms":
6: "Cinp:store input for next calculation":
7: "CVM:store output for next calculation":
8: "CVM??:store output for record,V(0)=V,N(0)=J":
9: "Cinp??:store input for record":
10: "Cnode:store input node information":
11: "Cnode?:permanent store input node information":
12: "Cnode-:temporary store  node information":
13: "CJ0:nodes for current calculation":
14: "CF:for c-A0 store temporary results":
15: "Nodes-inside start from 01 and increase":
16: "Nodes-boundary start from:0-1 and decrease":
17: "read and print start from left to right,top to bottom":
18: dsp "normalized dx and dy=1";wait 3000
19: dsp "no node on one side,insert zero";wait 3000
20: dsp "In case of symmetric";wait 3000
21: dsp "always make it N-S symmetric";wait 3000
22: dsp "and use north side for calculation";wait 3000
23: fxd 0;dim A0[3]
24: ent "total# of nodes=",T
25: ent "dx=",P;ent "dy=",Q;P=1e-5)P;Q=1e-5)Q
26: fmt c15,c10.3,c2
27: wrt 714,"dx=",P,"cm"
28: wrt 714,"dy=",Q,"cm"
29: ent "max. nodes in Y for calculation",Y
30: dim X[Y];dim R[Y+1]
31: dim Z0[1];dim V0[1];dim J[0:4];dim D[4];dim X0[3]
32: .72)U;6000)G;ent "doping=",N;1.6e-19/(12.5*8.85e-14)*N)M
33: ent "Change file Cnode?",A0
34: if cap(A0)="YES";gto "change node"
35: ent "S-symmetric or N-nonsymmetric",Z0
36: rread 1,1;sprt 1,Z0,"end"
37: gsb "title"
38: dsp "left to right,top to bottom";wait 2000
39: "ent":ent "node#",J[0]
40: if J[0]<0;J[0]).5;"B")V0
41: if J[0]>0;J[0])N;"I")V0
42: fxd 0;if J[0]>0;dsp "node inside #"&str(N);wait 3000;gto "1.5"
43: fxd 0;dsp "node-boundary #"&str(L);wait 3000
44: for K=1 to 4
45: 0)J[K])D[K]
46: next K
47: gto "2.5"
48: "1.5":if N=1 or N=2;jmp 3
49: ent "EVEN nodes shift=1?YES or NO",A0
50: if cap(A0)="YES";gto "shift"
51: ent "East node #",J[1]
52: ent "West node #",J[2]
53: ent "South node #",J[3]
54: ent "North node #",J[4]
55: "2":ent "Distances Same As Last One?",A0
56: if cap(A0)="YES";gto "3"
57: ent "dx(E)=",D[1]
58: ent "dx(W)=",D[2]
59: ent "dy(S)=",D[3]
60: ent "dy(N)=",D[4];gto "3"
61: "2.5":ent "(S)chottky?(O)hmic?",X0
62: ent "(F),(R)-biased?(O)rounded",X0[2]
63: "3":if cap(Z0)="N",X0[1,2])X0;jmp 3
64: ent "on symmetric axis? YES or NO",A0
```

```
65: if cap(A$)="YES";"Y")X$[3]
66: fmt f4.0,z;wrt 714,J[0]
67: if cap(Y$)="N";fmt 40z,z;wrt 714;gto "3.5"
68: fmt 8z,4f4.0,z;wrt 714,J[1],J[2],J[3],J[4]
69: wrt 714,D[1],D[2],D[3],D[4]
70: "3.5":fmt c25;wrt 714,cap(X$)
71: ent "Information is Correct?YES,NO",A$
72: if cap(A$)#"YES";gto "error"
73: "Copy Node Information":
74: sprt 1,Y$,J[M],D[M],X$,"end"
75: "   ")X$;if N-L-T;gto "prt"
76: gto "ent"
77: "prt":dsp "prt all node information";wait 3000
78: rread 1,1;sread 1,Z$;on end 1,"355"
79: gsb "title"
80: "S":sread 1,Y$,J[M],D[M],X$
81: fmt f4.0,z;wrt 714,J[0]
82: if J[0]<0;fmt c72;wrt 714,cap(X$);gto "S"
83: fmt 8z,4f4.0,z;wrt 714,J[1],J[2],J[3],J[4]
84: fmt 4z,4f5.2,z;wrt 714,D[1],D[2],D[3],D[4]
85: fmt c24;wrt 714,cap(X$)
86: gto "S"
87: "355":ent "Is all information correct?",A$
88: if cap(A$)="YES";gto "3.6"
89: gto "change node"
90: "3.6":fxd 0;dsp "Marking the leading Nodes";wait 2000
91: for I=1 to Y
92: dsp "Leading Node# on Line#"&str(I);wait 2000
93: ent R[I]
94: dsp "Node Position# on Line#"&str(I);wait 2000
95: ent X[I]
96: next I
97: rread 1,1;sread 1,Z$
98: on end 1,"6"
99: for I=1 to Y
100: for J=1 to X[I]
101: fmt c4,z;wrt 714,""
102: next J
103: if flg1;gto "5"
104: "4":sread 1,Y$,J[M],D[M],X$
105: if J[0]=R[I+1];sfg 1;fmt ;wrt 714;next I
106: "5":fmt f4.0,z;wrt 714,J[0];sfg 1
107: gto "4"
108: next I
109: "6":fmt /;wrt 714
110: ent "Anything Wrong in Printout? YES,NO",A$
111: if cap(A$)="YES";gto "3.6"
112: rread 2,1;sprt 2,P,Q,V,T,X[M],R[M],L,M,G,U,N,N,V,"end"
113: fmt c50;wrt 714,"Nodes for Current In and Out"
114: fmt 2,f6.0,4z,f6.0,c4,f8.4,15z,f6.0,4z,f6.0,c4,f8.4
115: rread 3,1
116: for I=1 to Y
117: "again":dsp "Line#"&str(I);wait 2000
118: ent "1st node on input",A
119: ent "2nd node on input",B
120: ent "normalized distance,#1&2 on input",C
121: ent "1st node on output",D
122: ent "2nd node on output",E
123: ent "normalized distance,#1&2 on output",F
124: wrt 714.2,A,B,"  d=",C,D,E,"  d=",F
125: ent "Something Wrong?YES,NO",A$
126: if cap(A$)="YES";fmt c50;wrt 714,"last line is wrong";gto "again"
127: sprt 3,A,B,C,D,E,F,"end"
128: next I
129: ent "Did you change Cnode?'?",A$
130: if cap(A$)#"YES";dsp "Change Cnode?";wait 3000;beep;stp
131: "8":copy "Cnode","node88"
132: get "chan2",0,0
```

```
133: "shift":for K=1 to 4
134: if J(K)<0;I=J(K)>J(K)
135: next K
136: gto "2"
137: "error":fmt c80;wrt 714,"error on last line"
138: "   ")X0;dsp "Don't Use Shift,Or ERROR!";wait 3000;gto "ent"
139: "change node":
140: rread 1,1;rread 4,1
141: sread 1,Z0
142: ent "change Z0?",A0
143: if cap(A0)="YES";ent "S or N",Z0
144: sprt 4,Z0,"end"
145: ent "correct only a part of nodes?",A0
146: if cap(A0)="YES";gsb "part"
147: ent "correct nodes?",A0
148: if cap(A0)="YES";gsb "correct"
149: ent "delect nodes?",A0
150: if cap(A0)="YES";gsb "delect"
151: ent "insert nodes?",A0
152: if cap(A0)="YES";gsb "insert"
153: ent "Def boundary nodes",L;-abs(L)>L
154: ent "Def inside nodes",M
155: gto "pri"
156: "title":fmt c80;if cap(Z0)="S";wrt 714,"Symmetric Geometry";jmp 2
157: wrt 714,"Nonsymmetric Geometry"
158: fmt c7,z;wrt 714,"node #"
159: fmt c21,z;wrt 714,"node in E.W.S.N"
160: fmt c24,z;wrt 714,"normalized distance"
161: fmt c35;wrt 714,"(S)chottky?(O)hmic?"
162: fmt c80;wrt 714,"(F),(R)-biased?(O)rounded?"
163: wrt 714,"on a(V)xmetric axis?"
164: ret
165: "correct":
166: rread 1,1;rread 4,1;sread 1,Z0;sprt 4,Z0,"end"
167: on end 1,"cr"
168: "c0":ent "correct nodes? if no more ent 0",J
169: "c1":sread 1,V0,J(M),D(M),X0
170: if J#J(0);sprt 4,V0,J(M),D(M),X0,"end";gto "c1"
171: ent "B or I",V0
172: ent "nodes?",J(0);if J(0)<0;gto "0"
173: for I=1 to 4
174: ent J(I);ent D(I)
175: next I
176: "0","   ")X0
177: for I=1 to 3
178: ent X0(I)
179: next I
180: sprt 4,V0,J(M),D(M),X0,"end";gto "c0"
181: "cr":copy "Gnode-","Gnode"
182: ret
183: "delect":
184: rread 1,1;rread 4,1;sread 1,Z0;sprt 4,Z0,"end"
185: on end 1,"dr"
186: "d0":ent "delect nodes-? if no more ent 0",J
187: "d1":sread 1,V0,J(M),D(M),X0
188: if J#J(0);sprt 4,V0,J(M),D(M),X0,"end";gto "d1"
189: gto "d0"
190: "dr":copy "Gnode-","Gnode"
191: ret
192: "insert":
193: rread 1,1;rread 4,1;sread 1,Z0;sprt 4,Z0,"end"
194: on end 1,"ir"
195: "i0":ent "last node-? if no more ent 0",J
196: "i1":sread 1,V0,J(M),D(M),X0
197: sprt 4,V0,J(M),D(M),X0,"end"
198: if J#J(0);gto "i1"
199: "i2":ent "nodes-?",J(0)
200: ent "B or I",V0;if J(0)<0;gto "i"
```

```
201: ent "shift J[m],D[m]?",A$
202: if cap(A$)#"YES";gto "101"
203: for I=1 to 4
204: J[I]=1)J[I]
205: if J[I]=0;0)J[I]
206: next I
207: gto "f"
208: "101":for I=1 to 4
209: ent J[I];ent D[I]
210: next I
211: "(","   ")X$
212: for I=1 to 3
213: ent X$[I]
214: next I
215: sprt 4,V$,J[m],D[m],X$,"end"
216: ent "one more next to it?",A$
217: if cap(A$)="YES";gto "12"
218: gto "10"
219: "1r":copy "Cnode-","Cnode"
220: ret
221: "part":
222: rread 1,1;rread 4,1;rread 1,Z$;sprt 4,Z$,"end"
223: on end 1,"pr"
224: "p$":ent "correct node#-?,if no more set 0",J
225: "p1":rread 1,V$,J[m],D[m],X$
226: if J#J[0];sprt 4,V$,J[m],D[m],X$,"end";gto "p1"
227: ent "node# is wrong?",A$
228: if cap(A$)="YES";ent J[0]
229: ent "J[?] is wrong?",A$
230: if cap(A$)="YES";ent J[1];ent J[2];ent J[3];ent J[4]
231: ent "D[?] is wrong?",A$
232: if cap(A$)="YES";ent D[1];ent D[2];ent D[3];ent D[4]
233: ent "X$ is wrong?",A$
234: if cap(A$)="YES","   ")X$;ent X$[1];ent X$[2];ent X$[3]
235: sprt 4,V$,J[m],D[m],X$,"end"
236: gto "p$"
237: "pr":copy "Cnode-","Cnode"
238: ret
m4814
```

Program 2 : Print Node Information

```
0: files Gnode
1: dim Z0[1];dim A0[3]
2: dim V0[1]
3: dim X0[3]
4: dim J[0:4]
5: dim D[4]
6: "prt":dsp "prt all node information";wait 3000
7: rread 1,1;rread 1,Z0;on end 1,"355"
8: gsb "title"
9: "S":rread 1,V0,J[=],D[=],X0
10: fmt f4.0,z;wrt 714,J[0]
11: if J[0]<0;fmt c72;wrt 714,cap(X0);gto "S"
12: fmt 8z,4f4.0,z;wrt 714,J[1],J[2],J[3],J[4]
13: fmt 4z,4f5.2,z;wrt 714,D[1],D[2],D[3],D[4]
14: fmt c24;wrt 714,cap(X0)
15: gto "S"
16: "title":fmt c50;if cap(Z0)="S";wrt 714,"Symmetric Geometry";jmp 2
17: wrt 714,"Nonsymmetric Geometry"
18: fmt c7,z;wrt 714,"node #"
19: fmt c21,z;wrt 714,"node in E.M.S.M"
20: fmt c24,z;wrt 714,"normalized distance"
21: fmt c38;wrt 714,"(S)chottky?(E)tmic?"
22: fmt c60;wrt 714,"(F),(N)-biased?(G)rounded?"
23: wrt 714,"on s(Y)mmetric axis?"
24: ret
25: "355":stp
```

Program 3 : Main Program

```
0: "chan2,drive0,6/2/81":
1: files Cmode,Cimp,CA,CAm,CAo,CVH,Cimp??,CVH00,CF,CJ0
2: rread 2,1;rread 2,P,G,V
3: dim X[V];dim R[V+1];cnt "Elmo.(G)?mat(1)?thin(2)?",r0
4: dim A0[3];1e-13>r1;afg 2
5: sread 2,T,X[=],R[=],L,N,G,U,H,N
6: dsp "Adjust Applied V.and dV";wait 1000
7: ent V;ent "dV",G;N1.6e-19/(12.5=0.85e-14)>N
8: rread 2,1;sprt 2,P,G,V,T,X[=],R[=],L,N,G,U,N,N,V
9: dim Z0[1];dim Y0[1];dim J[0:4];dim D[4];dim X0[3]
10: dim V[L:N];dim N[L:N];dim C[N];dim F[N];dim A[N,N]
11: if V=0;rread G,1;sread G,V[=],N[=]
12: "R":rread 2,1;sprt 2,P,G,V,T,X[=],R[=],L,N,G,U,N,N,V,"end"
13: rread 7,1;sprt 7,P,G,V,T,X[=],R[=],L,N,G,U,N,N,V,"end"
14: if V=0;ins V,N:1
15: rread 1,1;sread 1,Z0
16: on end 1,"1"
17: "B":sread 1,Y0,J[=],D[=],X0
18: J[0]>A;if A>0;gto "B"
19: X0[1,2]>A0;1/.0250>D
20: if cap(A0)="EF";exp(-VD)>N[A];V-U>V[A];if V<0;exp(VD)>N[A];-U>V[A]
21: if cap(A0)="ER";dsp "Wrong";stp
22: if cap(A0)="OF";exp(-VD)>N[A];V>V[A];if V<0;1>N[A];0>V[A]
23: if cap(A0)="OR";dsp "Wrong";stp
24: if cap(A0)="BO";exp(-BV)>N[A];-U>V[A];if V<0;exp(VD)>N[A];-V-U>V[A]
25: if cap(A0)="BO";1>N[A];0>V[A];if V<0;exp(VD)>N[A];-V>V[A]
26: gto "B"
27: "1":if V=0;gto "NR"
28: ins A,C,F;chain "s-AC",0,0
29: rread 3,1;sprt 3,A[=],"end"
30: inv A>A
31: mat AC>F
32: for I=1 to N
33: F[I]>V[I]
34: next I
35: "NR":ins A,C;rread 3,1;sread 3,A[=]
36: for I=1 to N
37: V[I]>C[I]
38: next I
39: mat AC>F
40: ins A,C;afg 0;chain "s-AC",0,0
41: sra F-C>F;rread 9,1;sprt 9,F[=],"end"
42: chain "s-AP",0,0
43: inv A>A
44: rread 9,1;sread 9,F[=]
45: "dV1":mat AF>C
46: 0>G
47: for I=1 to N
48: G+C[I]^2>G
49: next I
50: \(G/N)>G;fmt e15,e10.3;wrt 714,"dV1=",G
51: for I=1 to N
52: V[I]-C[I]>V[I]
53: next I
54: if V=0;gto "3"
55: ins A,C;chain "s-ACm",0,0
56: inv A>A;rread 4,1;sprt 4,A[=],"end"
57: mat AG>F
58: for I=1 to N
59: F[I]>N[I]
60: next I
61: rread G,1;sprt G,V[=],N[=],"end"
62: "3":if G>1e-3;gto "NR"
63: fmt e17,f10.3;wrt 714,"Applied Voltage=",V
64: chain "s-prt",0,0
```

```
65: 0int(V/0)+1)A;if 0<0;301-A)A
66: if int(V/0)<38;rread 0,A;sprt 0,V[M],N[M],"end"
67: rread 0,1;sprt 0,V[M],N[M],"end"
68: if N[0]>1e3;dsp "turn me off please";stp
69: 0+V)V
70: gto "R"
```

Program 4 : Coefficient Matrix for Poisson's Equation

```
0: "e-AC":
1: rread 1,1;sread 1,Z0
2: on and 1,"sret"
3: "s1":sread 1,V0,J[m],D[m],X0
4: if J[0]<0;gto "s1"
5: all "ee"(J[1],J[2],J[3],J[4],P0[1],P0[2],00[3],00[4],J[0])
6: gto "s1"
7: "sret":if V=0 or flg0;chain "chan2",0,41
8: chain "chan2",0,29
9: "ee":if p1p2=0;-2/p7p0)A[p0,p0);gsb "s3"
10: if p3p4=0;-2/p5p6)A[p0,p0];gsb "s2"
11: if p1p2p3p4=0;-2/p7p0-2/p5p6)A[p0,p0];gsb "s4"
12: gsb "K"
13: H(N[p0]exp(V[p0]K)-1)+C[p0])C[p0]
14: ret
15: "s2":2/p6/(p5+p6))A;if p2<0;-AV[p2])C[p0]
16: if p2=p0;A+A[p0,p0])A[p0,p0]
17: if p2>0 and p2<p0;A)A[p0,p2]
18: 2/p6/(p5+p6))B;if p1<0;C[p0]-BV[p1])C[p0]
19: if p1>0;B)A[p0,p1]
20: ret
21: "s3":2/p0/(p7+p0))A;if p4<0;C[p0]-AV[p4])C[p0]
22: if p4>0;A)A[p0,p4]
23: 2/p7/(p7+p0))B;if p3<0;C[p0]-BV[p3])C[p0]
24: if p3>0;A[p0,p3]+B)A[p0,p3]
25: ret
26: "s4":gsb "s2"
27: gsb "s3"
28: ret
29: "K":if r0=0;1/.0259)K;ret
30: 0)A)B
31: if p1p2<0;(V[p1]-V[p2])/(p5+p6))A
32: if p3p4<0;(V[p3]-V[p4])/(p7+p0))B
33: \(AA+BB))E;if r0=2;gto "\"
34: (8875+1.1e7(EEE/3200^4))/(1+(E/3200)^4))A
35: .0259A+2/3*r1*AE)B
36: A/B)K;ret
37: "\":if E<=3200;2e7/3200)A;.0259A+2/3*AE)B
38: if E>3200;2e7/E)A;.0259A+2/3*r1*2e7^2)B
39: A/B)K;ret
*E8700
```

Program 5 : Jacobian Matrix

```
0: "e-A0",
1: if V=0;gto "0"
2: "01":ima A,C;1/.0250/2)C
3: rread 1,1;sread 1,Z0
4: on end 1,"04"
5: "02":sread 1,V0,J[M],D[M],X0
6: if J[0]<0;gto "02"
7: all "03"(J[1],J[2],J[3],J[4],PD[1],PD[2],GD[3],GD[4],J[0])
8: gto "02"
9: "04":rread 5,1;sprt 5,A[M],"end"
10: if not flg2;rread 4,1;sread 4,A[M];jmp 3
11: ima A,C;sfg 3;cfg 2;chain "e-ACn",0,0
12: cfg 3;inv A)A
13: rread 5,1;rread 4,1
14: for I=1 to N
15: sread 5,F[M]
16: mat AF)C
17: sprt 4,C[M],"end"
18: next I
19: rread 4,1;sread 4,A[M]
20: rread 1,1;sread 1,Z0
21: for I=1 to N
22: sread 1,V0,J[M],D[M],X0
23: if J[0]#I;jmp -1
24: all "K"(J[1],J[2],J[3],J[4],PD[1],PD[2],GD[3],GD[4],J[0])
25: for J=1 to N
26: if J=I;N(A[J,I]-N(I)K)exp(V[I]K))A[J,I]
27: if J#I;NA[J,I]exp(V[I]K))A[J,I]
28: next J
29: next I
30: rread 3,1
31: for I=1 to N
32: sread 3,F[M]
33: for J=1 to N
34: A[J,I]-F[J])A[J,I]
35: next J
36: next I
37: chain "chan2",0,43
38: "0":ima C;rread 1,1;sread 1,Z0
39: for I=1 to N
40: sread 1,V0,J[M],D[M],X0
41: if J[0]#I;jmp -1
42: all "K"(J[1],J[2],J[3],J[4],PD[1],PD[2],GD[3],GD[4],J[0])
43: A[I,I]-NKexp(V[I]K))A[I,I]
44: next I
45: chain "chan2",0,43
46: "03":for I=1 to 4
47: I+4)J;if pI-p0;gto "00"
48: if pI<=0;gto "00"
49: if r0=0;0exp(GV[pI])/pJN(N[p0]-N[pI]))A[p0,pI]
50: if r0=1;gsb "031"
51: "00":next I
52: rat
53: "K":if r0=0;1/.0250)K;rat
54: 0)A)B
55: if pIp2=0;(V[pI]-V[p2])/(p5-p6))A
56: if p3p4=0;(V[p3]-V[p4])/(p7-p8))B
57: \(AA-BB))E;if r0=2;gto "\1"
58: (8875+1.1e7(EEE/3200^4))/(1+(E/3200)^4))A
59: .0250A+2/3=v1=A(AE)B
60: A/B)K;rat
61: "\1":if E<=3200;2e7/3200)A;.0250A+2/3=v1=A(AE)B
62: if E>3200;2e7/E)A;.0250A+2/3=v1=2e7^2)B
63: A/B)K;rat
64: "031",
```

```
65: gsb "B"
66: (N[p0]-N[p1])F/2*exp(B(V[p1]+V[p0])/2)/pJ)Z
67: Z+A[p0,p0])A[p0,p0]
68: Z)A[p0,p1]
69: ret
70: "B":abs((V[p1]-V[p0])/pJ))E;if r0=2;gto "\2"
71: (8875+1.1e7(EEE/3200^4))/(1+(E/3200)^4))F
72: .0259F+2/3*r1*EFEF)D
73: F/D)B;ret
74: "\2":if E<-3200;2e7/3200)F;.0259F+2/3*r1EFEF)D
75: if E)3200;2e7/E)F;.0259F+2/3*r1*2e7^2)D
76: F/D)B;ret
*14318
```

Program 6 : Coefficient Matrix for Current Equation

```
0: "c-ACn":1/.0259/2)A
1: rread 1,1;sread 1,Z$
2: on end 1,"ret"
3: "n1":sread 1,Y$,J(=),D(=),X$
4: if J(0)<0;gto "n1"
5: cll 'an'(J(1),J(2),J(3),J(4),PD(1),PD(2),QD(3),QD(4),J(0))
6: gto "n1"
7: "ret":if flg3;chain "c-A$",0,12
8: chain "chan2",0,56
9: "an":
10: for I=1 to 4
11: if pI=p9;gto "p"
12: if pI=0;gto "p"
13: I+4)J;gsb "B"
14: if pI<0;C(p9)+BH(pI))C(p9)
15: A(p9,p9)+B)A(p9,p9)
16: if X$="" or X$="  ";jmp 2
17: if cap(X$[3])="Y" and I=4 and pI>0;-2B)A(p9,p4];gto "p"
18: if pI>0;-B)A(p9,pI)
19: "p":next I
20: ret
21: "B":if r0=0;exp(AV(pI))/pJ)B;ret
22: abs((V(pI)-V(p9))/pJ))E;if r0=2;gto "\"
23: (6875+1.1e7(EEE/3200^4))/(1+(E/3200)^4))F
24: .0259F+2/3=r1EFEF)D
25: "DF":D/pJ=exp(F/D/2=(V(p9)+V(pI))))B
26: ret
27: "\":if E<-3200;2e7/3200)F;.0259F+2/3=r1EFEF)D
28: if E>3200;2e7/E)F;.0259F+2/3=r(1)2e7^2)D
29: gto "DF"
=2770
```

Program 7 : Printout Results

```
0: "c-prt":fmt c3,e10.4,c2,4x,c3,e10.4,c6,e10.2
1: wrt 714,"dx=",P,"cm","dy=",Q,"cm  N=",N
2: if r0=0;fmt c10,f5.0;wrt 714,"mobility=",G
3: fmt c50;if r0=0;wrt 714,"Einstein Relation"
4: if r0=1;wrt 714,"Generalized Mobility and Velocity"
5: if r0=2;wrt 714,"Thin Layer Mobility and Velocity"
6: fmt c20,e10.2,c3;if r0#0;wrt 714,"Relax. time=",r1,"sec"
7: ins C,F;1)A)B;cfg 1
8: rread 1,1;sread 1,Z$
9: "w1":sread 1,Y$,J[M],D[M],X$
10: J[0])C[A];if A<M;A+1)A;gto "w1"
11: on end 1,"w3"
12: "w2":sread 1,Y$,J[M],D[M],X$
13: J[0])F[B];B+1)B;gto "w2"
14: "w3":fmt c10;wrt 714,"V1="
15: 1)A
16: rread 1,1;sread 1,Z$
17: for I=1 to Y
18: gsb "space"
19: gsb "VM"
20: next I
21: 1)A;cfg 1;fmt ;wrt 714,""
22: if Z$="S";fmt c60;wrt 714,"Last line is Symmetric Axis"
23: fmt c10;wrt 714,"N1=";0)X
24: rread 1,1;sread 1,Z$
25: for I=1 to Y
26: gsb "space"
27: gsb "VM"
28: next I
29: cfg 1
30: fmt ;wrt 714,""
31: if Z$="S";fmt c60;wrt 714,"Last Line is Symmetric Axis"
32: "Capacitance":1.6e-19*N(T-X))X
33: fmt c20,e13.6;wrt 714,"total charge=",X
34: "Current":fmt /;wrt 714
35: rread 10,1
36: fmt c16,34x,c20;wrt 714,"Current dens. in","Current dens. out"
37: fmt 1,e11.3,42x,e11.3
38: 0)S)M
39: for I=1 to Y
40: sread 10,A,B,C,D,E,F
41: if r0=0;gto "J1"
42: cll 'JK'(A,B,PC,J)
43: cll 'JK'(D,E,PF,K)
44: gto "SM"
45: "J1":exp((V[A]+V[B])/.0259/2)/CP*(N[B]-N[A])*G*.0259*1.6e-19)J
46: exp((V[D]+V[E])/.0259/2)/FP*(N[E]-N[D])*G*.0259*1.6e-19)K
47: "SM":S+J)S;M+K)M
48: wrt 714.1,J,K
49: next I
50: fmt c40;wrt 714,"Average Current Dens."
51: if cap(Z$)="N";gto "p1"
52: S-J/2)S;M-K/2)M;wrt 714.1,S/(Y-.5),M/(Y-.5)
53: (S+M)/2(Y-.5))N[0];V)V[0]
54: gto "p2"
55: "p1":wrt 714.1,S/Y,M/Y
56: (S+M)/2Y)N[0];V)V[0]
57: "p2":chain "chan2",0,65
58: "space":
59: for J=1 to X[1]
60: fmt c8,z;wrt 714,""
61: next J
62: rat
63: "VM":if A>M;F[A-M])B;jmp 2
64: C[A])B
```

```
65: if B=R[I+1];fmt ;wrt 714;ret
66: fmt f8.5,z;if not flg1;wrt 714,V[B];gto "T"
67: if r0=0 or B<0;N[B]exp(V[B]/.0258)}J;wrt 714,J;gto "T"
68: gsb "K"
69: N[B]exp(KV[B]))J;wrt 714,J
70: "T":J+X}X;if A=T;ret
71: A+1}A;gto "VW"
72: "JK":abs((V[p1]-V[p2])/p3)}r2;if r0=2;gto "\1"
73: (6875+1.1e7(r2^3/3200^4))/(1+(r2/3200)^4)}r3
74: .0259r3+2/3*r1(r2r3)^2}r4
75: "p4":1.6e-19*r4*exp(r3/r4/2*(V[p1]+V[p2]))/p3*(N[p2]-N[p1]))}p4
76: ret
77: "\1":if r2<=3200;2e7/3200}r3;.0259r3+2/3*r1(r2r3)^2}r4
78: if r2>3200;2e7/r2}r3;.0259r3+2/3*r1*2e7^2}r4
79: gto "p4"
80: "K":
81: "ir":sread 1,V0,J[=],D[=],X0
82: if J[0]#0;gto "ir"
83: cll "Ni"(J[1],J[2],J[3],J[4],PD[1],PD[2],GD[3],GD[4],J[0])
84: "2r":ret
85: "Ni":0}Z}M
86: if p1p2#0;(V[p1]-V[p2])/(p5+p6)}M
87: if p3p4#0;(V[p3]-V[p4])/(p7+p8)}Z
88: \(MM+ZZ)}E;if r0=2;gto "\2"
89: (6875+1.1e7(EEE/3200^4))/(1+(E/3200)^4)}F
90: .0259F+2/3*r1*EFEF}D
91: F/D}K;ret
92: "\2":if E<=3200;2e7/3200}F;.0259F+2/3*r1EFEF}D
93: if E>3200;2e7/E}F;.0259F+2/3*r1*2e7^2}D
94: F/D}K;ret
*12567
```

9. BIBLIOGRAPHY

1. H. Gummel, "A self-consistent iterative scheme for one-dimensional steady-state transistor calculations," IEEE Transactions on Electron Devices, FD-11, pp. 455-465, October 1964.

2. D. McCumber and A. Chynoweth, "Theory of negative-conductance amplification and of Gunn instabilities in two-valley semiconductors," IEEE Transactions on Electron Devices, ED-13, pp. 4-21, January 1966.

3. A. De Mari, "An accurate numerical steady-state one-dimensional solution of the p-n junction," Solid State Electronics, Vol. 11, pp. 33-58, January 1968.

4. B. Gokhale, "Numerical solutions for a one-dimensional silicon n-p-n transistor," IEEE Transactions on Electron Devices, ED-17, pp. 594-602, August 1970.

5. V. Arandjelovic, "Accurate numerical steady-state solutions for a diffused one-dimensional junction diode," Solid State Electronics, Vol. 13, pp. 865-871, 1970.

6. G. Hachtel, R. Joy and J. Cooley, "A new efficient one-dimensional analysis program for junction device modelling," Proceedings of the IEEE, Vol.60 pp. 86-98, January 1972.

7. T. Seidman and S. Choo, "Iterative scheme for computer simulation of semiconductor devices," Solid State Electronics, Vol. 15, pp.1229-1235, 1972.

8. J. Slotboom, "Computer aided two-dimensional analysis of bipolar transistor," IEEE Transactions on Electron Devices, ED-20, pp. 669-679, August 1973.

9. D. Kennedey and R. O'Brien, "Electric current saturation in a junction field-effect transistor," Solid State Electronics, Vol. 12, pp. 829-830, August 1969.

10. P. Dubock, "Numerical analysis of forward and reverse bias potential distribution in a two-dimensional p-n junction with applications to capacitance calculations," Electronics Letters, Vol. 5, pp. 236-238, May 1969.

11. E. Wasserstrom and J. McKenna, "The potential due to a charged metallic strip on a semiconductor surface," The Bell System Technical Journal, Vol.49, pp. 853-877, May 1970.

12. C. Kim and E. Yang, "An analysis of current saturation mechanism of junction field-effect transistors," IEEE Transactions on Electron Devices, E-17, pp.120-127, February 1970.

13. M. Reiser and P. Wolf, "Computer study of submicrometre F.E.T.s," Electronics Letters, Vol. 8, pp. 254-256, April 1972.

14. M. Reiser, "Large-scale numerical simulation in semiconductor device modelling," Computer Methods in Applied Mechanics and Engineering, Vol. I, pp.17-39, April 1973.

15. M. Reiser, "A two-dimensional numerical FET model for dc, ac, and large signal analysis," IEEE Transactions on Electron Devices, Vol. 20, pp. 35-45, January 1973.

16. M. Reiser, "On the stability of finite difference schemes in transient semiconductor problems," Computer Method in Applied Mechanics and Engineering, Vol.2, pp. 65-68, 1973.

17. D. Vandorpe and N. Xuong, "Mathematical two-dimensional model of semiconductor devices," Electronics Letters, Vol. 7, pp. 47-50, January 1971.

18. D. Vandorpe, J. Barel, G. Merckel and P. Saintot, "An accurate two-dimensional numerical analysis of the MOS transistor," Solid State Electronics. Vol. 15, pp. 547-557, 1972.

19. M. Mock, "A two-dimensional mathematical model of the insulated field-effect transistor," Solid State Electronics, Vol. 16, pp.601-609, 1973.

20. K. Yamaguchi and H. Kodera, "Drain conductance of junction gate FET's in the hot electron range," IEEE Transactions on Electron Devices, ED-23, pp. 545-553, June 1976.

21. E. Buturla and P. Cottrell, "Two-dimensional finite element analysis of semiconductor steady-state transport equations," International Conference on Computational Methods in Nonlinear Mechanics, Austin, Texas, 1974.

22. G. Hachtel, M. Mack and R. O'Brien, "Semiconductor device analysis via finite elements," Eighth Asilomar Conference on Circuits and Systems, Pacific Grove, California, pp. 332-338, 1974.

23. P. Cottrell and E. Buturla, "Steady state analysis of field effect transistors via the finite element method," Digest of the IEEE International Electron Devices Meeting Washington, D.C., pp 51-54, December 1975.

24. J. Barnes and R. Lomax, "Finite-element methods in semiconductor device simulation," IEEE Transactions on Electron Devices, ED-24, pp. 1082-1089, 1977.

25. T. Adachi, A. Yoshii and T. Sudo, "Two-dimensional semiconductor analysis using finite-element method," IEEE Transactions on Electron Devices, ED-26, pp. 1026-1031, 1979.

26. E. Buturla, P. Cottrel, B. Grossman and K. Salsburg, "Finite-element analysis of semiconductor devices: the FIELDAY program," IBM Journal on Research and Development, Vol. 25, pp. 218-231, July 1981.

27. G. Hachtel, M. Mack, R. O'Brien and B. Speelpenning, "Semiconductor analysis using finite elements - part I: Computational aspects, part II: IGFET and BJT case studies," IBM Journal on Research and Development, pp. 232-260, July 1981

28. E. Buturla, P. Cottrell, B. Grossman, M. Lawlor, C. McMullen and K. Salsburg, "Three dimensional simulation of semiconductor devices," IEEE International Solid State Circuits Conference Digest of Technical Papers, San Francisco, pp. 76-77, February 1980.

29. M. Reiser, "Computing methods in semiconductor problems," IBM research report, RJ 1343, January 1974, private communication.

30. O. Zienkiewicz, The Finite Element Method, 3 rd edition, McGraw-Hill, chapter 18, 1977.

31. H. Watson, Microwave Semiconductor Devices and Their Circuit Applications, McGraw-Hill, chapter 11, 1969.

32. B. Henderson, "Mixers: part I and part II," Tech-notes, Watkins-Johnson, Palo Alto, California, 1981.

33. M. Howes and D. Morgan, "Variable impedance devices," John Wiley & Sons, chapter 2 and 4, 1978.

34. G. Robinson, "Metalurgical ane electrical properties of alloyed Ni/Au-Ge films on n-type GaAs," Solid State Electronics, Vol. 18, pp. 331-342, 1975.

35. C. Brucker and L. Brillson, "New method for control of Schottky-barrier height," Applied Physics Letter, Vol. 39, pp. 67-69, July 1981.

36. R. Malik, K. Board, L. Eastman, C. Wood, T. AuCoin, R. Ross and R. Savage, "GaAs planar doped barriers by molecular beam epi-taxy," IEDM Technical Digest, pp. 456-459, 1980.

37. S. Teng, P. Chen, F. Rosenbaum and R. Goldwasser, "The Gap diode: A new high frequency mixer and detector," IEEE MTT's International Microwave Symposium, Dallas, Texas, June 1982.

38. M. Cohn, J. Degenford and B. Newman, "Harmonic mixing with an anti-parallel diode pair," IEEE MTT's International Microwave Symposium Digest, pp. 171-172, June 1974.

39. E. Rhoderick, Medul-Semiconductor Contact, Clarendon Press, Oxford, 1978.

40. S. Sze, Physics of Semiconductor Devices, John Wiley & Sons, chapter 8, 1969.

41. A. van der Ziel, Solid State Physical Electronics, 3 rd edition, Prentice-Hall, chapter 14, 1976.

42. B. Streetman, Solid State Electronic Devices, Prentice-Hall, chapter 5, 1972.

43. P. Bulman, G. Hobson and B. Taylor, Transferred Electron Devices, Academic Press, chapter 3, 1972.

44. H. Thim, "Computer study of bulk GaAs devices with random one-dimensional doping fluctuations," Journal of Applied Physics, Vol. 39, pp. 3897-3904, July 1968.

45. K. Yamaguchi, T. Toyabe and H. Kodera, "Effect of Field-dependent carrier diffusion on the two-dimensional analysis of a Junction gate FET," Japan Journal of Appplied Physics, Vol. 14, pp. 1069-1070, 1975.

46. H. Grubin, D. Ferry and J. Barker, "Transient effects in submicron devices- load line dependence," private communication, 1979.

47. B. Browne and J. Miller, (editors), Numerical Analysis of Semiconductor Devices, Boole Press, Dublin, Ireland, pp. 3-21 and 32-64, 1979.

48. M. Schneider and W. Snell, "Stripline downconverter with subharmonic pump," Bell System Technical Journal, Vol. 53, pp. 1179-1183, 1974.

49. A. Kerr, "Noise and loss in balanced and subharmonically pumped mixers: part I and part II," IEEE Transactions on Microwave Theory and Techniques, MTT-27, pp. 938-950, December 1979.

50. A. Cardiasmenos, "New diodes cut the cost of millimeter-wave mixers," Microwaves Journal, pp. 78-88, September 1978.

51. E. Stoneham, "The search for the fastest three-terminal device," Microwaves Journal, pp. 55-65, February 1982.

DISTRIBUTION LIST
CONTRACT N00014-79-C-0840

Code 414 — 4
Office of Naval Research
Arlington, VA 22217

Naval Research Laboratory
4555 Overlook Avenue, S.W.
Washington, D.C. 20375
Code 6811 — 1
6850 — 1
6820 — 1
6851 — 1

Defense Documentation Center — 12
Building 5, Cameron Station
Alexandria, VA 22314

Dr. Y. S. Park — 1
AFWAL/DHR
Building 450
Wright-Patterson AFB
Ohio 45433

Texas Instruments — 1
Central Research Lab
M.S. 134
13500 North Central Expressway
Dallas, TX 75265
ATTN: Dr. W. Wisseman

Dr. R. M. Malbon/M.S. 1C — 1
Avantek, Inc.
3175 Bowers Avenue
Santa Clara, CA 94304

Dr. R. Bierig — 1
Raytheon Company
28 Seyon Street
Waltham, MA 02154

Dr. Mike Driver — 1
Westinghouse Research and
Development Center
Beulah Road
Pittsburgh, PA 15235

Dr. F. Eisen — 1
Rockwell International
Science Center
P.O. Box 1085
Thousand Oaks, CA 91360

Dr. C. Krumm — 1
Hughes Research Laboratory
3011 Malibu Canyon Raod
Malibu, CA 90265

Mr. Lothar Wandinger — 1
ECOM/AMSEL/TL/IJ
Fort Monmouth, NJ 07003

Dr. William Lindley — 1
MIT
Lincoln Laboratory
F124 A, P.O. Box 73
Lexington, MA 02173

Commander — 1
U.S. Army/ERADCOM
ATTN: V. Gelnovatch, DELET-M
Fort Monmouth, NJ 07703

RCA — 1
Microwave Technology Center
Dr. F. Sterzer
Princeton, NJ 08540

Commander — 1
Naval Electronics Systems Command
ATTN: J. P. Letellier, Code 6142
Washington, D.C. 20360

Commander — 1
Naval Air Systems Command
ATTN: A. Glista, Jr., AIR 34
Washington, D.C. 20361

Dr. R. Bell, K-101 — 1
Varian Associates, Inc.
611 Hansen Way
Palo Alto, CA 94304

Hewlett-Packard Corporation 1
Dr. Robert Archer
1501 Page Road
Palo Alto, CA 94306

Watkins-Johnson Company 1
E. J. Crescenzi, Jr./
K. Niclas
3333 Hillview Avenue
Stanford Industrial Park
Palo Alto, CA 94304

Commandant 1
Marine Corps
Scientific Advisor (Code AX)
Washington, D.C 20380

Communications Transistor Corp. 1
Dr. W. Weisenberger
301 Industrial Way
San Carlos, CA 94070

Microwave Associates 1
Northwest Industrial Park
Drs. F. A. Brand/J. Saloom
Burlington, MA 01803

Commander, AFAL 1
AFWAL/AADM
Dr. Don Rees
Wright-Patterson AFB, OH 45433

Professor Walter Ku 1
Phillips Hall
Cornell University
Ithaca, NY 14853

Commander 1
Harry Diamond Laboratories
Mr. Horst W. A. Gerlach
800 Powder Mill Road
Adelphia, MD 20783

A.G.E.D. 1
201 Varick Street
9th Floor
New York, NY 10014

Dr. Ken Weller 1
MS/1414
TRW Systems
One Space Park
Redondo Beach, CA 90278

Professor L. Eastman 1
Phillips Hall
Cornell University
Ithaca, NY 14853

Professor Hauser and 1
Littlejohn
Department of Electrical Engr.
North Carolina State University
Raleigh, NC 27607

Professor J. Beyer 1
Department of Electrical and
Computer Engineering
University of Wisconsin
Madison, WI 53706

W. H. Perkins 1
Electronics Lab 3-115/B4
General Electric Company
P.O. Box 4840
Syracuse, NY 13221

Bryan Hill 1
AFWAL/AADE
Wright-Patterson AFB, OH 45433

H. Willing/Radar Directorate 1
BMD - Advanced Technical Center
P.O. Box 1500
Huntsville, AL 35807

END

FILMED